The Astrophysical Journal Supplement Series, 197:28 (34pp), 2011 December doi:10.1088/0067-0049/197/2/28

AN H I SURVEY OF SIX LOCAL GROUP ANALOGS. II. H I PROPERTIES OF GROUP GALAXIES

D. J. Pisano[1,7], David G. Barnes[2], Lister Staveley-Smith[3], Brad K. Gibson[4,5], Virginia A. Kilborn[2], and Ken C. Freeman[6]
[1] Department of Physics, West Virginia University, P.O. Box 6315, Morgantown, WV 26506, USA; djpisano@mail.wvu.edu
[2] Centre for Astrophysics and Supercomputing, Swinburne University, Hawthorn, Victoria 3122, Australia; David.G.Barnes@gmail.com, vkilborn@astro.swin.edu.au
[3] International Centre for Radio Astronomy Research, M468, University of Western Australia, Crawley, WA 6009, Australia; Lister.Staveley-Smith@icrar.org
[4] Jeremiah Horrocks Institute, University of Central Lancashire, Preston PR1 2HE, UK; brad.k.gibson@gmail.com
[5] Department of Astronomy and Physics, Saint Mary's University, Halifax, Nova Scotia B3H 3C3, Canada
[6] RSAA, Mount Stromlo Observatory, Cotter Road, Weston, ACT 2611, Australia; kcf@mso.anu.edu.au
Received 2011 September 2; accepted 2011 October 13; published 2011 November 29

ABSTRACT

We have conducted an H I 21 cm emission-line survey of six loose groups of galaxies chosen to be analogs to the Local Group. The survey was conducted using the Parkes multibeam instrument and the Australia Telescope Compact Array (ATCA) over a $\sim$1 Mpc^2 area and covering the full depth of each group, with an $M_{\rm H\,I}$ sensitivity of $\sim 7 \times 10^5\ M_\odot$. Our survey detected 110 sources, 61 of which are associated with the six groups. All of these sources were confirmed with ATCA observations or were previously cataloged by HIPASS. The sources all have optical counterparts and properties consistent with dwarf irregular or late-type spiral galaxies. We present here the H I properties of the groups and their galaxies. We derive an H I mass function (HIMF) for the groups that is consistent with being flatter than the equivalent field HIMF. We also derive a circular velocity distribution function, tracing the luminous dark matter halos in the groups, that is consistent with those of the Local Group and HIPASS galaxies, both of which are shallower than that of clusters or predictions from cold dark matter models of galaxy formation.

Key words: galaxies: evolution – galaxies: formation – galaxies: groups: general – galaxies: luminosity function, mass function – Local Group

Online-only material: color figures

1. INTRODUCTION

The majority of galaxies, including the Milky Way, reside in groups (Geller & Huchra 1983; Tully 1987; Eke et al. 2004; Tago et al. 2008), as such it is essential to study these structures if we wish to understand the effect of the environment on galaxy properties. A galaxy group is a very broad classification that has not been very precisely defined in the literature and whose properties span a wide range of mass and density (amongst others). They range in size from massive, rich groups to low-mass poor, loose groups and compact groups. The rich groups tend to be dominated by early-type galaxies (Postman & Geller 1984; Helsdon & Ponman 2003) and have an X-ray bright, intra-group medium (IGM; Mulchaey 2000; Mulchaey et al. 2003) that may result in ram pressure stripping of gas-rich spiral galaxies (Sengupta & Balasubramanyam 2006; Sengupta et al. 2007). In these ways, rich groups are very similar to low-mass galaxy clusters. Compact groups are the densest groups with a range of masses, containing a few to tens of galaxies typically separated by only a couple of galaxy radii (e.g., Hickson 1982, 1997). These groups contain galaxies that are strongly interacting and can also host an X-ray bright IGM (Ponman et al. 1996) potentially generated by the tidal interactions of the group members (Verdes-Montenegro et al. 2001).

In contrast to both of these classes, loose, poor groups are similar to the Local Group. They are less massive than rich groups, although with similar numbers of member galaxies. They can be dominated by either late-type or early-type galaxies, but only the groups containing at least one early-type galaxies have a hot, X-ray emitting IGM (Mulchaey 2000; Mulchaey et al. 2003). This suggests that ram pressure stripping is unlikely to have a large effect on galaxies in most of these groups (cf. Grcevich & Putman 2009). These groups are diffuse with low velocity dispersions resulting in crossing times that are comparable to a Hubble time and, as such, they are unlikely to be virialized (Zabludoff & Mulchaey 1998). This implies that interactions are rare, but, due to the low velocity dispersions, are more effective than in clusters and rich groups. These interactions may even strip H I from galaxies in loose, poor groups (Omar & Dwarakanath 2005).

While there have been a number of studies of the gaseous properties of isolated galaxies (Haynes & Giovanelli 1984; Pisano & Wilcots 1999; Pisano et al. 2002), of cluster galaxies (e.g., Bravo-Alfaro et al. 2000, 2001; Chung et al. 2009), and of compact and rich groups (e.g., Williams & Rood 1987; Williams et al. 1991; Verdes-Montenegro et al. 2001; Freeland et al. 2009; Kilborn et al. 2009; Borthakur et al. 2010), there have been fewer targeted studies of poor, loose groups analogous to our own Local Group. This paper seeks to fill that gap by exploring the neutral hydrogen properties of galaxies in six nearby, loose groups.

Mass functions serve as an excellent test of models of galaxy formation and are a simple of way quantifying differences between galaxy populations in different environments and comparing observations with models (Snaith et al. 2011). Current models of cold dark matter (CDM) galaxy formation predict an excess of low mass, as parameterized by their circular

[7] Adjunct Assistant Astronomer at National Radio Astronomy Observatory, P.O. Box 2, Green Bank, WV 24944, USA.

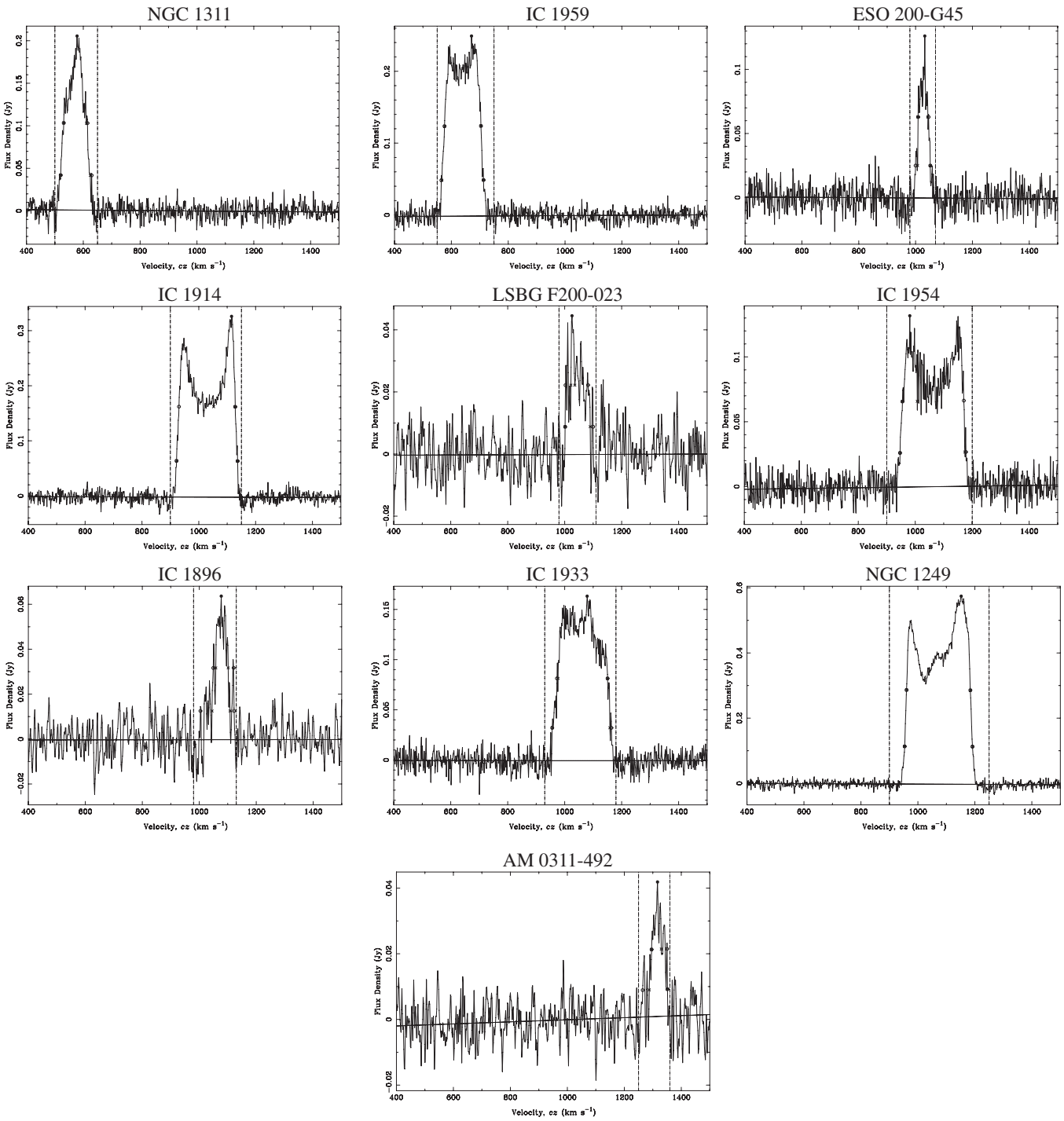

Figure 1. Parkes H I spectra of the confirmed detections in LGG 93. The vertical dashed lines indicate the range of velocities over which the profile properties were measured. The filled circles indicate the peak of the profile; the open circles the maximum 20% and 50% velocity widths; the ×'s mark the minimum 20% and 50% widths. The nearly horizontal solid line indicates the baseline fit to the spectrum.

velocity (the circular velocity distribution function, CVDF), dark matter halos as compared to what is observed locally (Klypin et al. 1999; Moore et al. 1999). While some authors have directly measured the CVDF for luminous galaxies (e.g., Shimasaku 1993; Sheth et al. 2003; Goldberg et al. 2005), this is difficult to do for very low mass dwarf galaxies; Blanton et al. (2008) and others have used different methods to infer the CVDF or used alternative proxies. The optical luminosity function has been regularly used as a proxy (e.g., Tully et al. 2002; Trentham et al. 2005) for the CVDF. Luminosity functions can also be used in concert with the Tully–Fisher relation or fundamental plane to infer the CVDF (Cole & Kaiser 1989; Gonzalez et al. 2000; Sheth et al. 2003; Desai et al. 2004; Goldberg et al. 2005). Unlike optical luminosity functions, using radio observations of 21 cm emission from neutral hydrogen (H I) provides two measures of the mass of a galaxy: the integrated line profile yields the H I mass while the linewidth provides the circular rotation velocity of the galaxy. Regardless of how the halo mass function is measured, be it by optical luminosity (Tully et al. 2002; Trentham et al. 2005), H I mass (Zwaan et al.

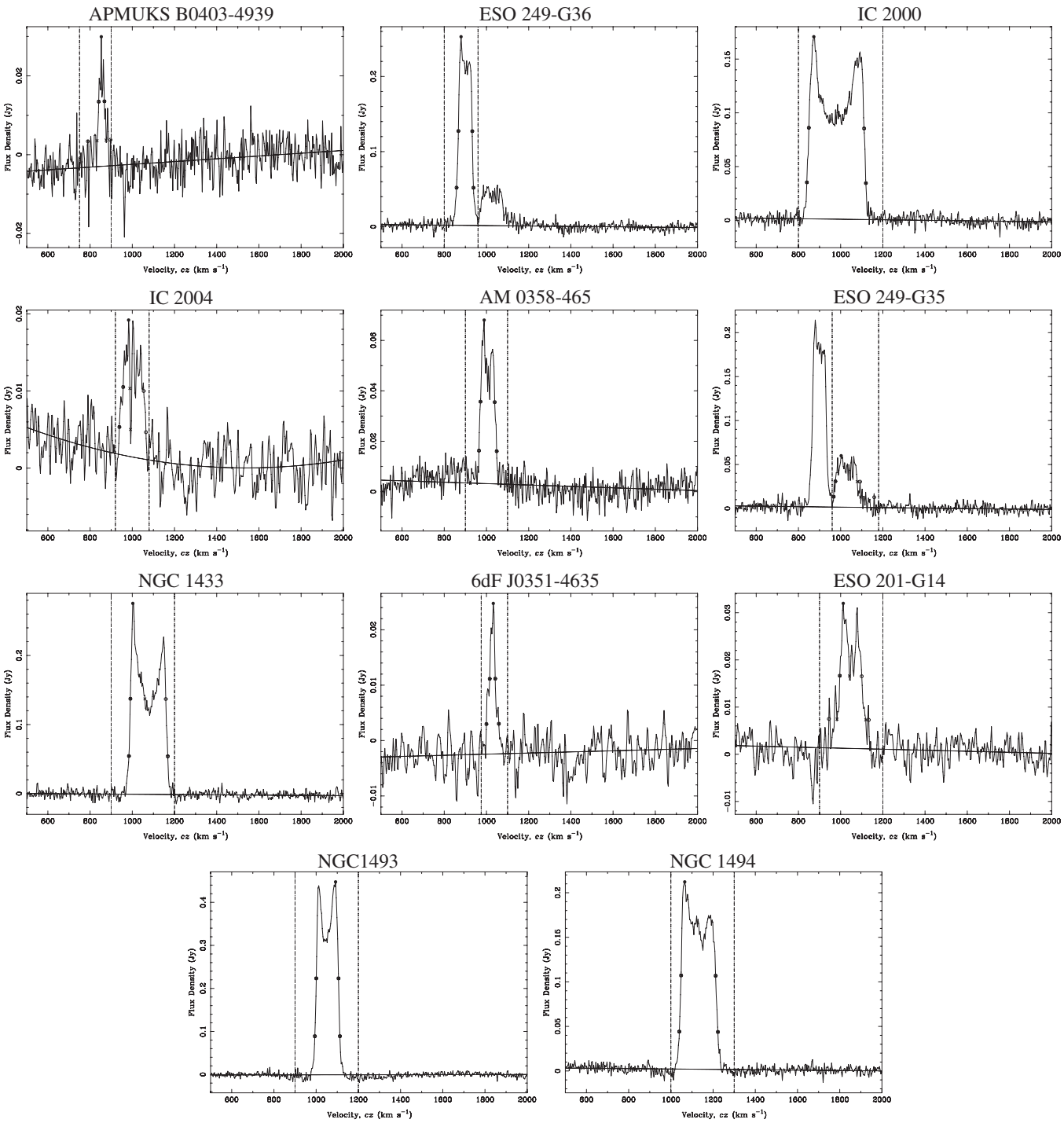

Figure 2. Same as Figure 1, but for LGG 106 group galaxies.

2005), or circular velocity (Zwaan et al. 2010), there is always a deficit of observed galaxies at low masses; this is the "missing satellite" or "substructure" problem (Klypin et al. 1999; Moore et al. 1999). Furthermore, there have been relatively few studies of how the H I mass function (HIMF) and CVDF may vary with environment. In this paper, we will compare the HIMF and CVDF for our six loose groups with those of the galaxy population in general and in other specific environments.

This is the second of two papers concerning our survey. In the first paper (Pisano et al. 2007, hereafter Paper I), we described our selection criteria, survey parameters, observations, data reduction, and the survey goals. These will be briefly summarized in this paper. We have already used our data to place constraints on the amount of intra-group H I clouds that may be analogous to the high-velocity clouds (HVCs; Wakker & van Woerden 1997) seen around the Milky Way. Namely, that any such HVC analogs must reside within 90 kpc of galaxies and have a total $M_{\rm H\,I} \lesssim 10^8\,M_\odot$ (Pisano et al. 2004; Paper I). In this paper, we will discuss the reliability of our survey and data analysis, present our H I data on the galaxies in the six groups, derive an HIMF and CVDF for the loose group environment, and discuss the implications for the effect of environment

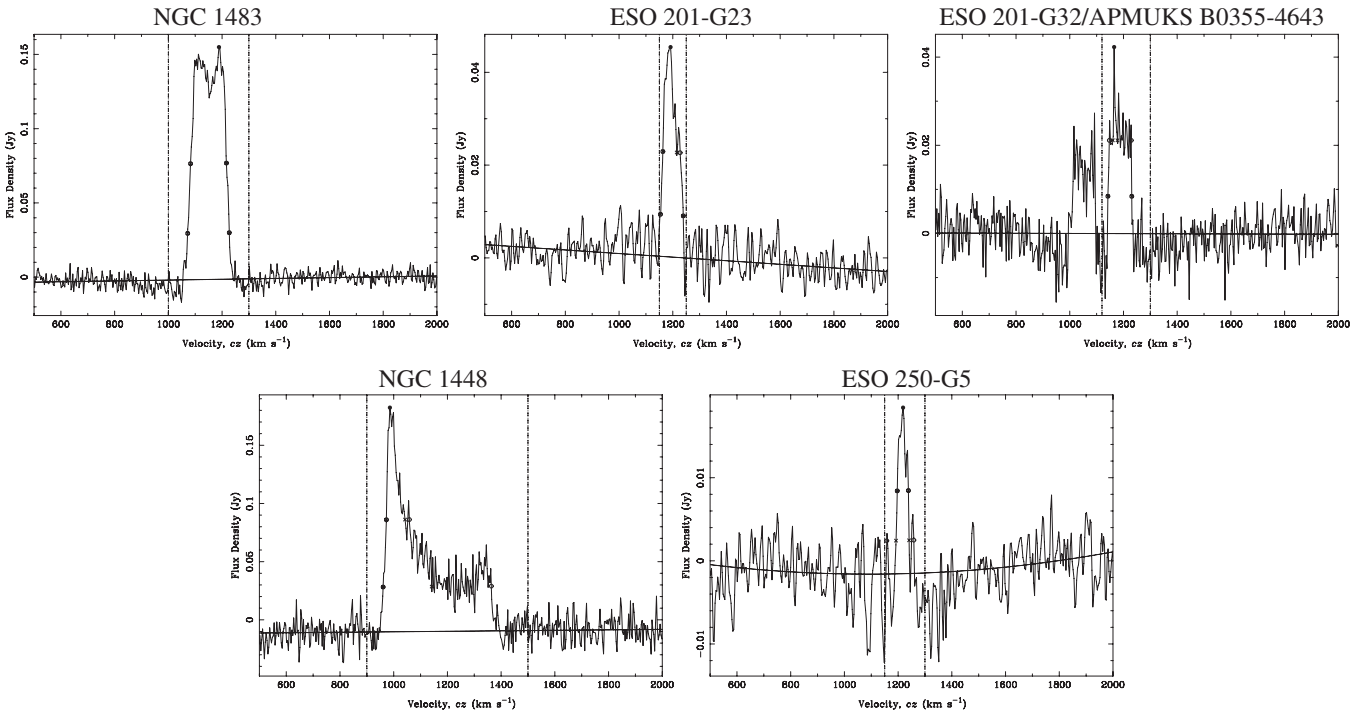

Figure 3. Same as Figure 1, but for the remaining LGG 106 group galaxies.

on galaxy formation. We summarize the sample selection in Section 2 and the observations and data reduction in Section 3. The results are presented in Section 4 including a description of the reliability and completeness of the survey, how we measure the galaxy properties, and a summary of the group and galaxy properties. Finally, we present the HIMF in Section 5, the CVDF in Section 6, and our conclusions in Section 7.

2. SAMPLE SELECTION

For this project, we identified six poor, loose groups of galaxies that are analogous to the Local Group. Details are given in Paper I, but the selection is summarized here. Groups were selected to be nearby ($v_{\rm GSR} < 1000$ km s^{-1}), but not confused with Galactic H I emission ($v_{\rm GSR} > 300$ km s^{-1}). The groups only contain spiral or irregular galaxies separated, on average, by a few hundred kiloparsecs with a total extent of $\sim$1 Mpc. Because our observations were made with the Parkes radio telescope in Australia, we only chose groups below a declination of 0°. We selected five groups, LGG 93, LGG 106, LGG 180, LGG 293, and LGG 478, from the Lyon Groups of Galaxies (LGG) catalog of Garcia (1993) and a sixth group from the HICAT group catalog of Stevens (2005). Distances are corrected using the multi-attractor velocity flow model of Masters (2005; K.L. Masters 2010, private communication), and assuming $H_0 = 72$ km s^{-1} Mpc^{-1} (Spergel et al. 2003). The measured properties of the groups are discussed in detail in Section 4.3.

3. OBSERVATIONS AND DATA REDUCTION

We observed the entire extent of the six groups between 2001 October and 2003 June using the 20 cm multibeam instrument (Staveley-Smith et al. 1996) on the Parkes 64 m radio telescope.[8] Observations of the first two groups, LGG 93 and LGG 180, were made with an 8 MHz bandwidth and 1.65 km s^{-1} channels using the inner seven beams of the multibeam, while all subsequent observations were made using all 13 beams, a 16 MHz bandwidth, and 3.3 km s^{-1} channels. All groups were observed only at night to avoid solar interference. Maps were made by scanning in a basket-weave pattern in right ascension and declination with consecutive scans being offset to result in uniform coverage perpendicular to the scan direction. Data were calibrated using periodic observations of flux calibrator Hydra A with a resulting accuracy of about 10%. All data were reduced and gridded using the LIVEDATA and GRIDZILLA packages. The 1σ, 3.3 km s^{-1} rms noise in these cubes range from 5.5 to 7.0 mJy, corresponding to an $M_{\rm H\,I}$ of (3.5–11) $\times$ 10^5 $M_\odot$ and $N_{H\,\rm I}$ of (2.8–4.6) $\times$ 10^{16} cm^{-2} depending on the group. For a 5σ detection of a source with a 30 km s^{-1} linewidth, we have an $M_{\rm H\,I}$ limit of (0.5–2) $\times$ 10^7 $M_\odot$, and an $N_{H\,\rm I}$ limit of (4.2–6.9) $\times$ 10^{17} cm^{-2}. It is worth noting that our reduction technique will subtract out sources that are larger than a few beams across.

The final cubes were searched by three groups of authors: D.J.P., D.G.B., and B.K.G. and V.A.K. in tandem. Our final list of putative sources included those that were identified by at least two of the three groups of authors. In addition, our identification of fake sources added to our cubes by M. Zwaan allowed us to assess the completeness of our survey, as discussed in Paper I.

We used the Australia Telescope Compact Array (ATCA)[9] to confirm the reality of the sources identified in our Parkes data. We observed 105 of the 112 Parkes detections in and behind the six groups in our sample. The remaining seven

[8] The Parkes radio telescope is part of the Australia Telescope National Facility which is funded by the Commonwealth of Australia for operation as a National Facility managed by CSIRO.

[9] The Australia Telescope is part of the Australia Telescope National Facility which is funded by the Commonwealth of Australia for operation as a National Facility managed by CSIRO.

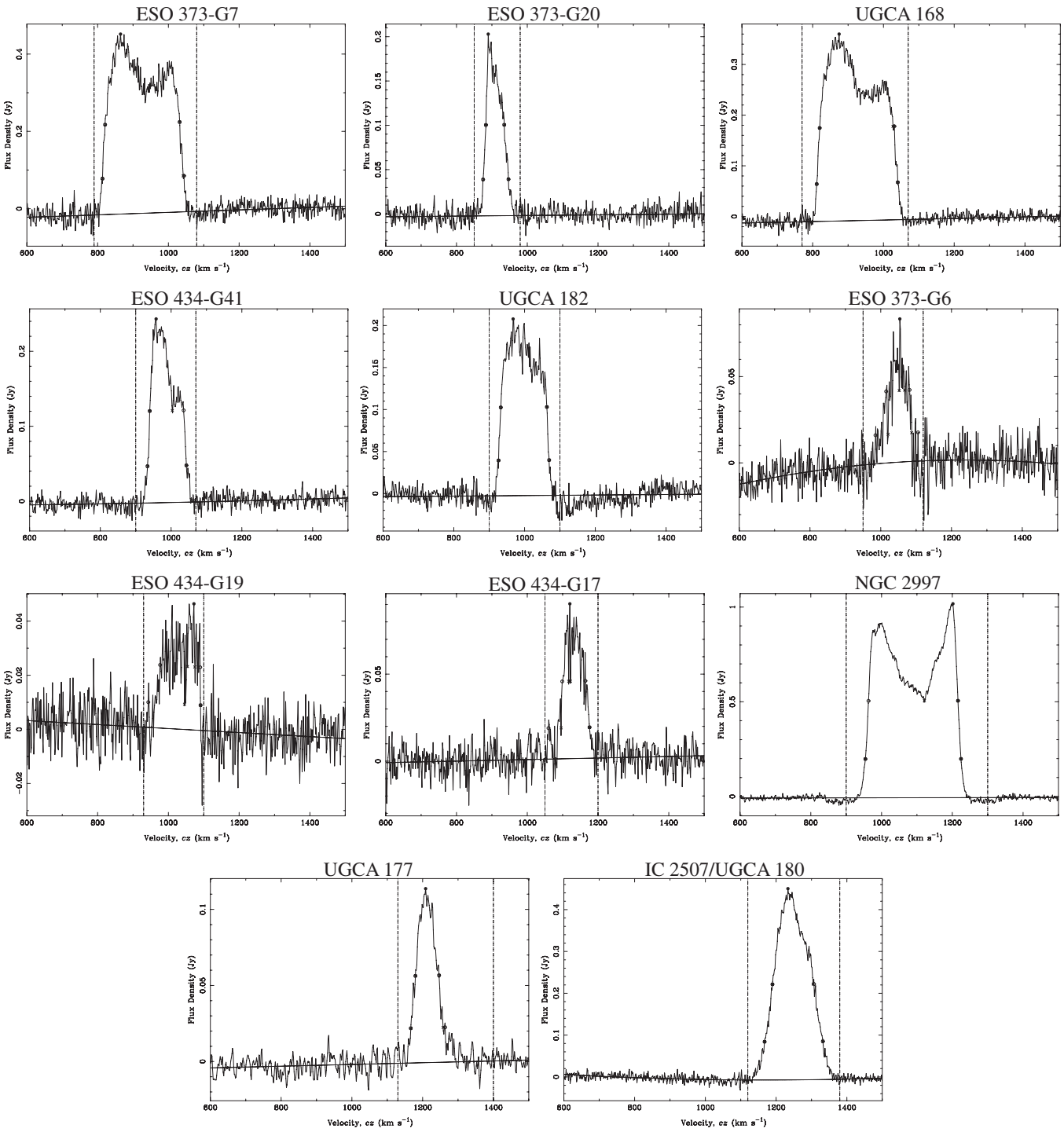

Figure 4. Same as Figure 1, but for LGG 180 group galaxies.

galaxies were all behind the groups and previously detected by HIPASS (Meyer et al. 2004). Of the 105 sources, 15 had previously been observed with the ATCA or Very Large Array (VLA) with similar resolution and equal or better sensitivity than our original observations. Data cubes for IC 1959, ESO 348-G9, IC 5332, ESO 249-G35, ESO 249-G36, IC 2000, NGC 5084, and ESO 576-G40 came from project C 934 courtesy of Emma Ryan-Weber. Data for NGC 2997 comes from the Giant Metreware Radio Telescope (GMRT) and ATCA and were discussed in detail in Hess et al. (2009). The remaining archival data was taken from the ATCA or VLA archives and re-reduced. The galaxies and projects with archival ATCA data are as follows: ESO 347-G29 (C073), NGC 1433 (C305), NGC 1448 (C295, C419), IC 1986 (C631, C942), UGCA 289 (C1046), NGC 5068 (C892), and ESO 575-G61 (C894). Those with VLA data are DDO 146 (AD474) and UGCA 320 (AC320).

We observed the remaining 90 sources between 2002 October and 2005 March using a compact configuration with baselines shorter than 750 m yielding beams of $\sim 1'$–$2'$, with the exception of galaxies toward the equatorial group LGG 293. For those sources we used the H214C configuration, which utilizes the north spur of the ATCA and has a maximum baseline of 214 m

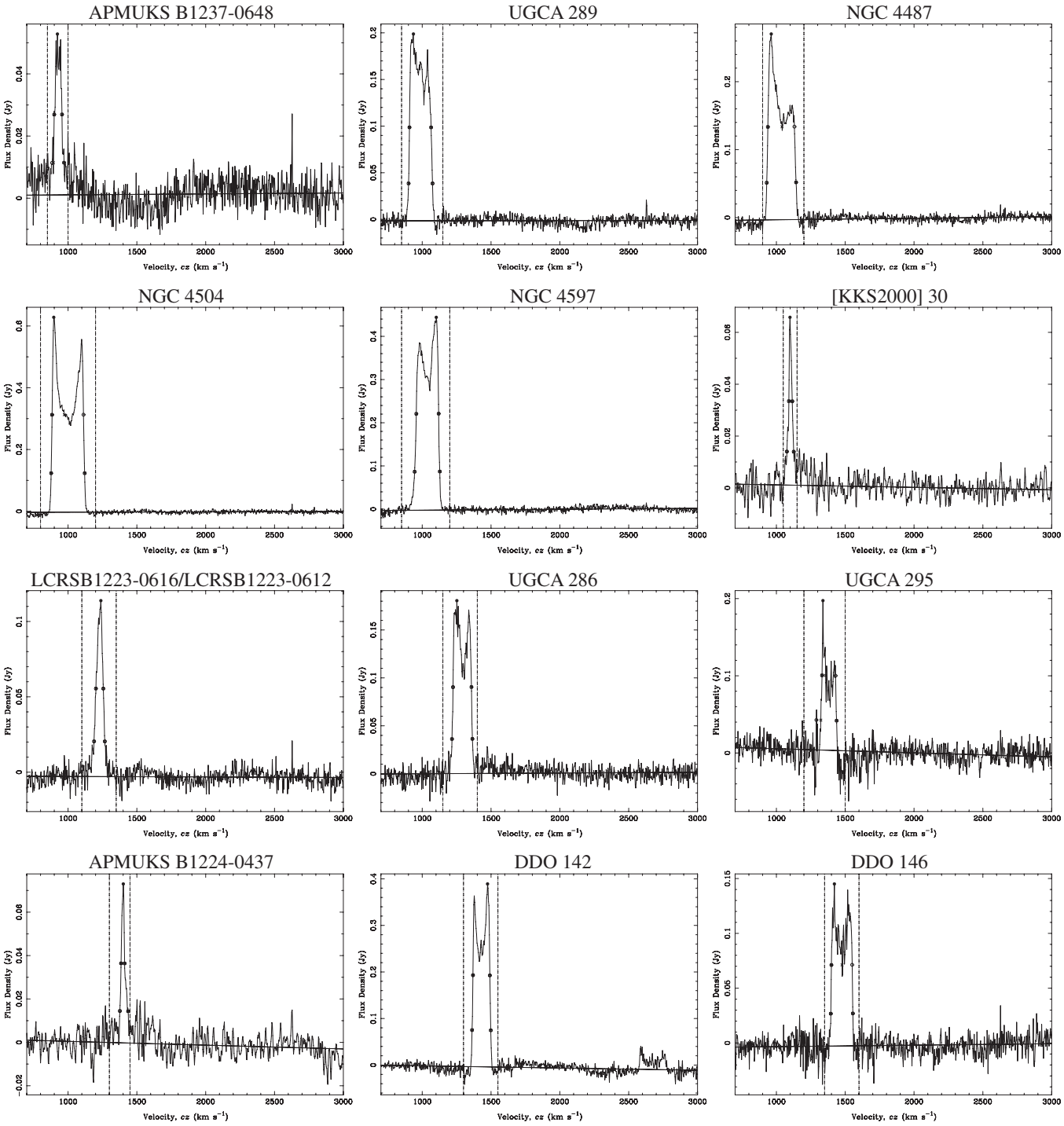

Figure 5. Same as Figure 1, but for LGG 293 group galaxies.

producing a beam of ∼2′–3′. Sources were observed to at least the same point-source sensitivity as the Parkes observations, ∼4 mJy beam^{-1}.

More details on all the observations, data reduction, and source-finding can be found in Paper I.

4. SURVEY RESULTS

4.1. Reliability and Completeness

Our ATCA observations served two purposes. The primary purpose was to establish the reality of the putative Parkes detections, while the secondary purpose was to identify any H I-rich galaxies that were confused at the Parkes resolution. Our original and archival interferometer observations confirmed the reality of 106 Parkes detections and revealed an additional four dwarf galaxies behind the target groups that were confused in the original Parkes data. As such our current sample of 110 H I-rich galaxies is 100% reliable.

The completeness, which is a necessary measure of a survey if one wishes to construct mass functions, is far more complicated and is discussed in detail in Paper I. Figure 3 of Paper I shows the completeness as a function of the linewidth and integrated signal-to-noise ratio of the source based on the fake sources that were inserted into our Parkes data cubes. In Paper I, we

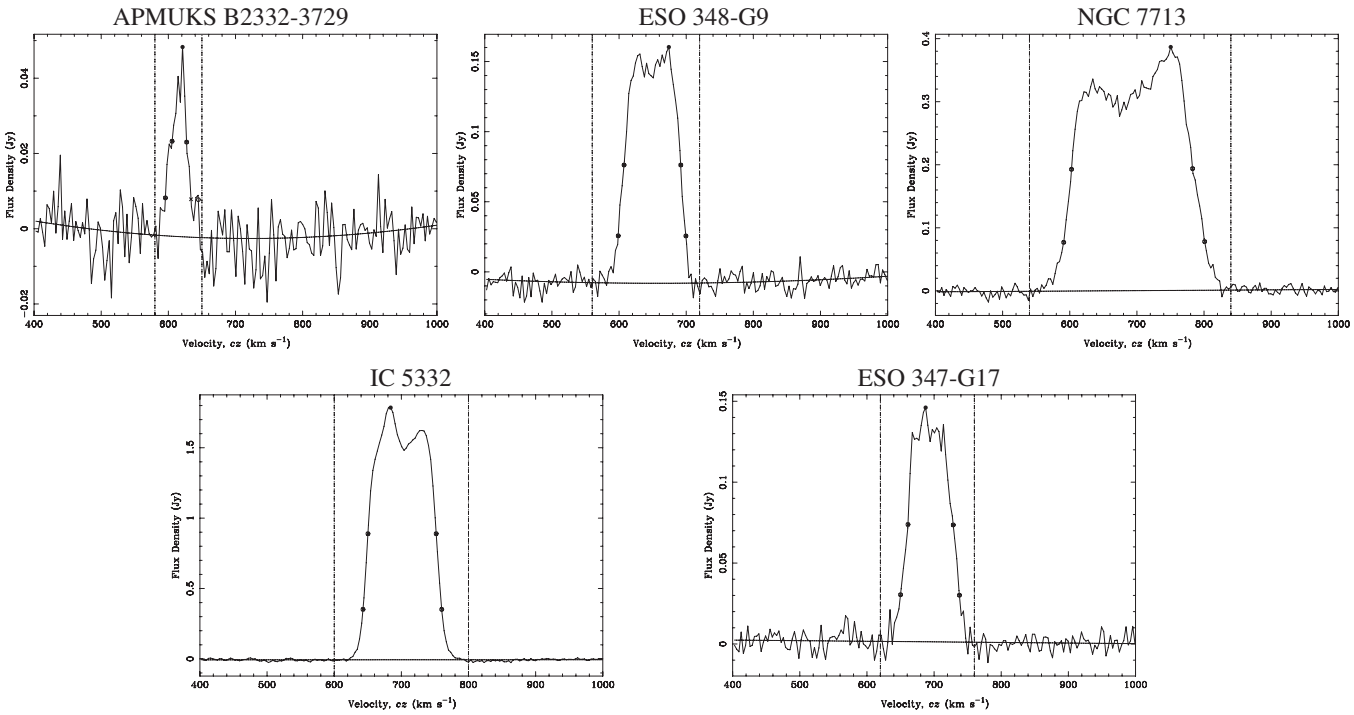

Figure 6. Same as Figure 1, but for LGG 478 group galaxies.

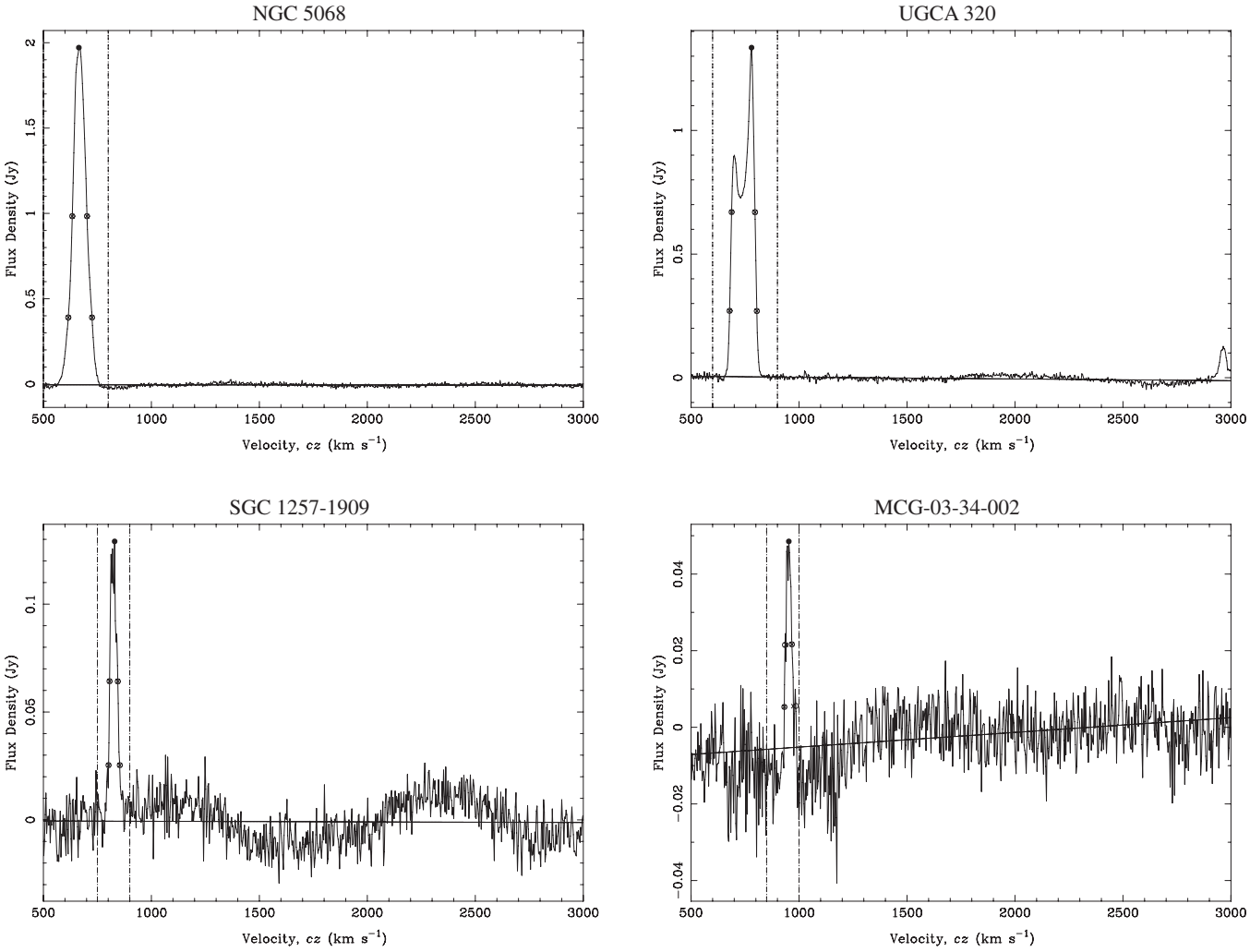

Figure 7. Same as Figure 1, but for HIPASS group galaxies.

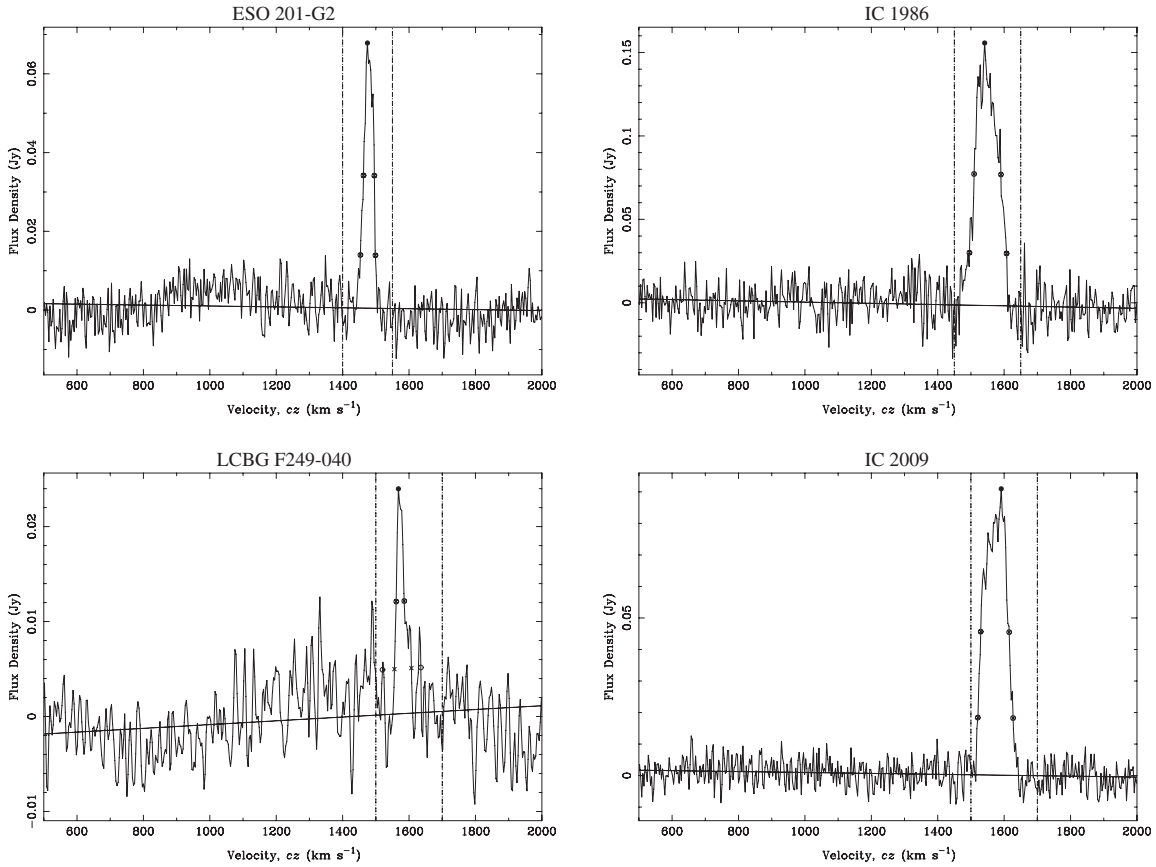

Figure 8. Same as Figure 1, but for galaxies behind LGG 106.

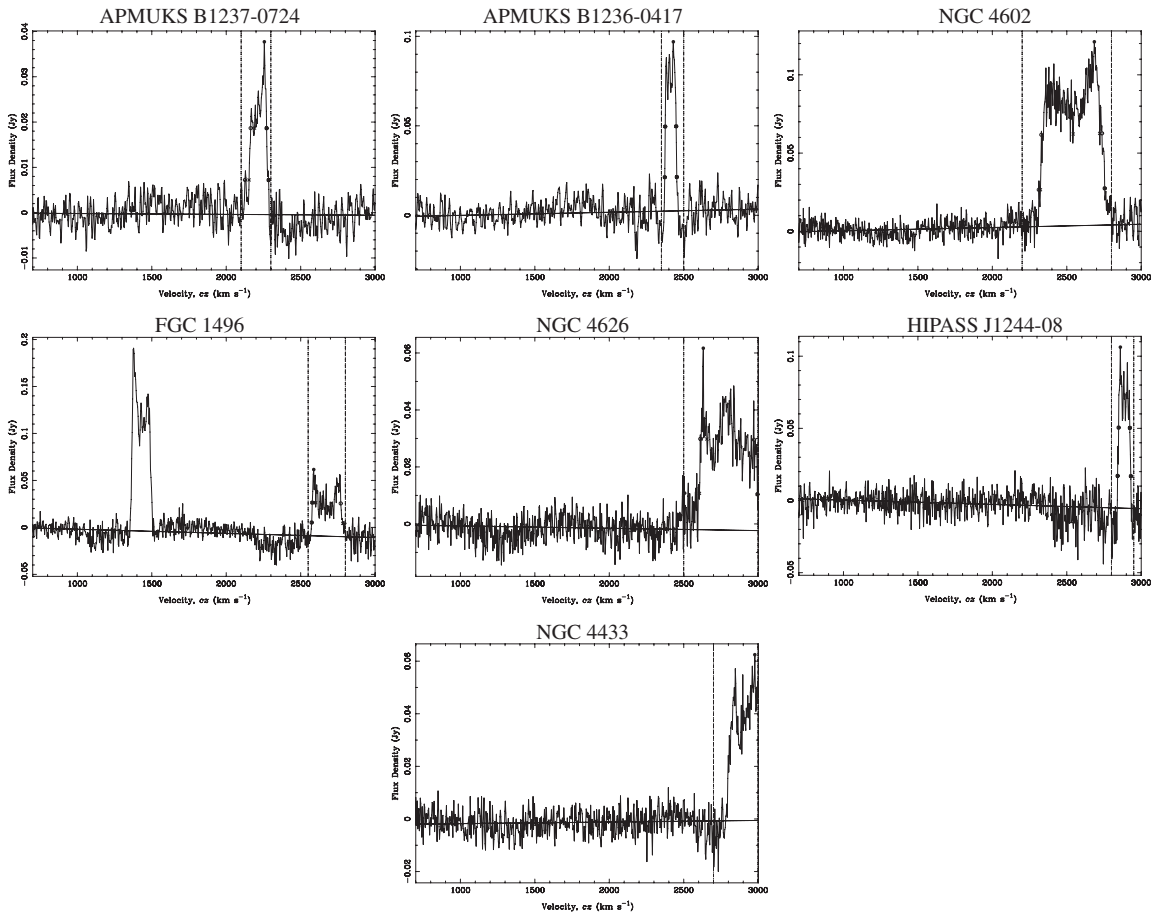

Figure 9. Same as Figure 1, but for galaxies behind LGG 293.

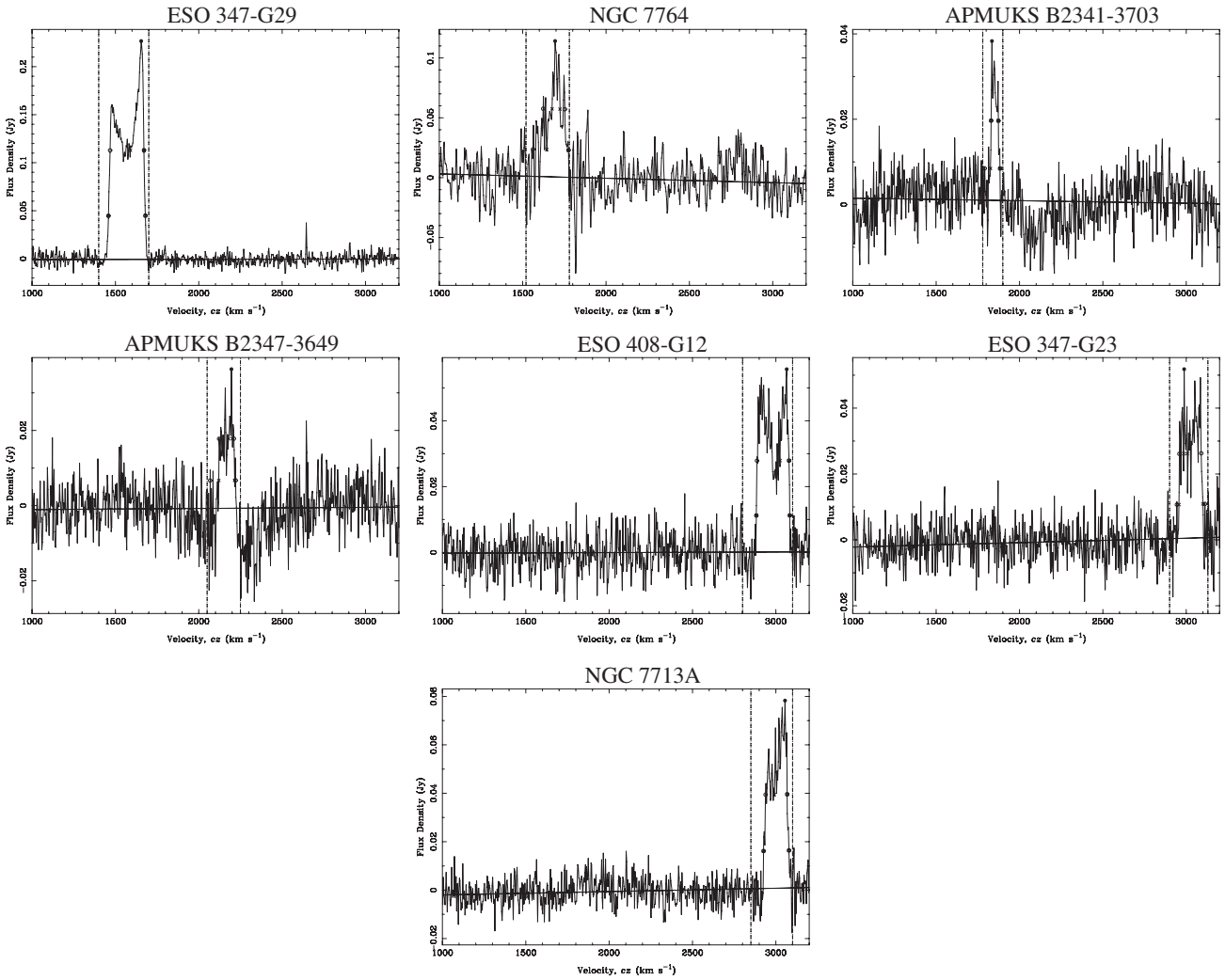

Figure 10. Same as Figure 1, but for galaxies behind LGG 478.

showed that the completeness we inferred was well described by the completeness function for HIPASS from Zwaan et al. (2004) after adjusting it for the different channel widths and noise levels of the two surveys. As in Paper I, we use that scaled completeness function in this paper to derive the HIMF and CVDF.

4.2. Measuring Galaxy Properties

Basic source parameters, such as position, recessional velocity, integrated H I flux, and linewidth were measured from the Parkes data using the MBSPECT task in MIRIAD. While searching the cubes, initial positions and velocities were determined for each source. Using MBSPECT, we inspected the cube at these positions to determine a velocity range to fit a first- or a second-order spectral baseline (for any residual shape not removed in the reduction process). MBSPECT takes an input position and velocity and a range of velocities to fit a baseline and measure the H I profile. It then creates a moment map over the latter range and fits a Gaussian to determine the central position of the source. MBSPECT then forms the spectrum in a $28' \times 28'$ box centered at this position. For weak sources, the spectra are Hanning smoothed. The resulting spectrum is then robustly integrated and the velocity width at the first and last crossings of 20% of the peak flux are identified. Typically, we chose the maximum width here, but when this was corrupted by noise spikes, the minimum or an average of the minimum and maximum width was chosen instead. For the two galaxies behind LGG 293 that are at the edge of the observed band, we can only achieve lower limits or highly uncertain estimates of the linewidth and integrated fluxes. The Parkes H I spectra of all detections, including indications of the peak flux as well as the 50% and 20% crossings, are shown in Figures 1–12. Where there were multiple galaxies within the Parkes beamwidth, we used the ATCA data to measure the galaxy properties. This was done in the same fashion, except the position was fixed on the known location of the emission and the box in which the line was measured was defined to tightly enclose the visible emission.

We can estimate the errors for our measured parameters by comparing real and measured values for the detected fake sources (see Paper I for details on the fake sources) and by comparing our measured parameters with those in HICAT (Meyer et al. 2004). For the fake sources, our position uncertainty is $2'$. For the remainder of the parameters, after discarding pathological outliers (more than 10σ, discussed below), V, W_{20}, and $S_{\rm int}$ show a scatter of 2 km s^{-1}, 4 km s^{-1}, and 0.3 Jy km s^{-1}, respectively. This is much better than the errors for HICAT (Zwaan et al. 2004), even though our fake sources also tend to be fainter, on average, than Zwaan et al.'s. For those sources with large discrepancies, they are mostly faint sources where noise spikes

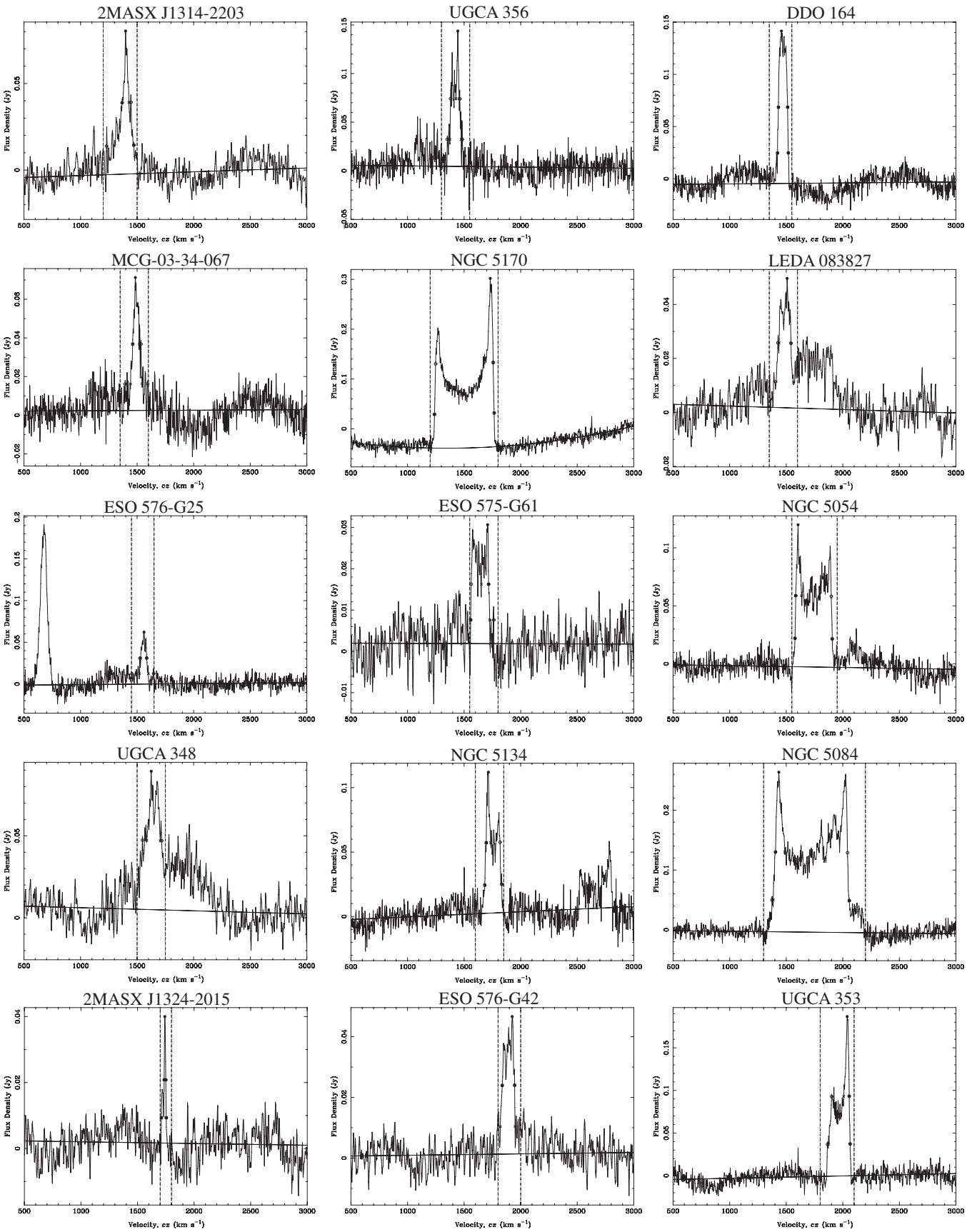

Figure 11. Same as Figure 1, but for galaxies behind the HIPASS group.

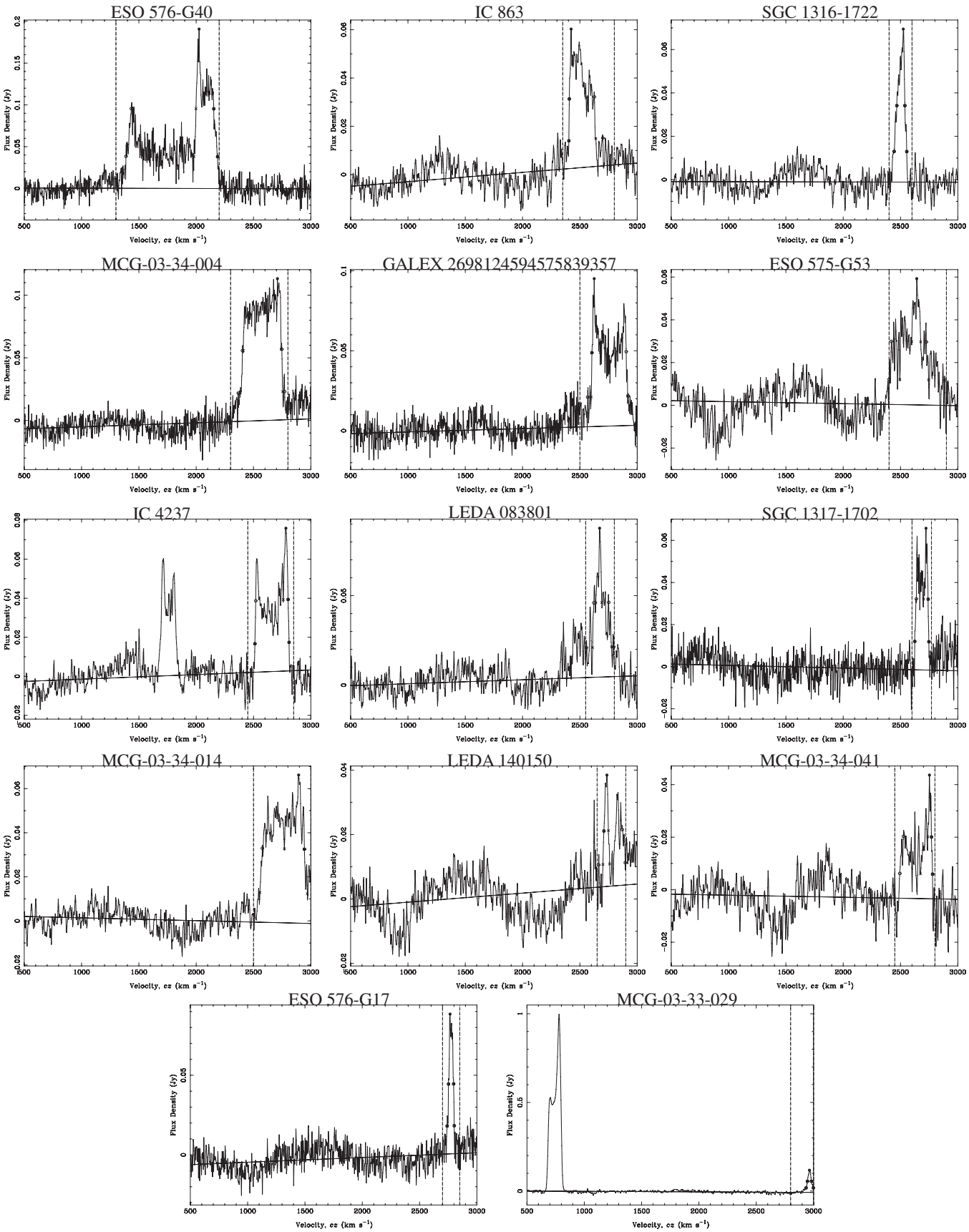

Figure 12. Same as Figure 1, but for the remaining galaxies behind the HIPASS group.

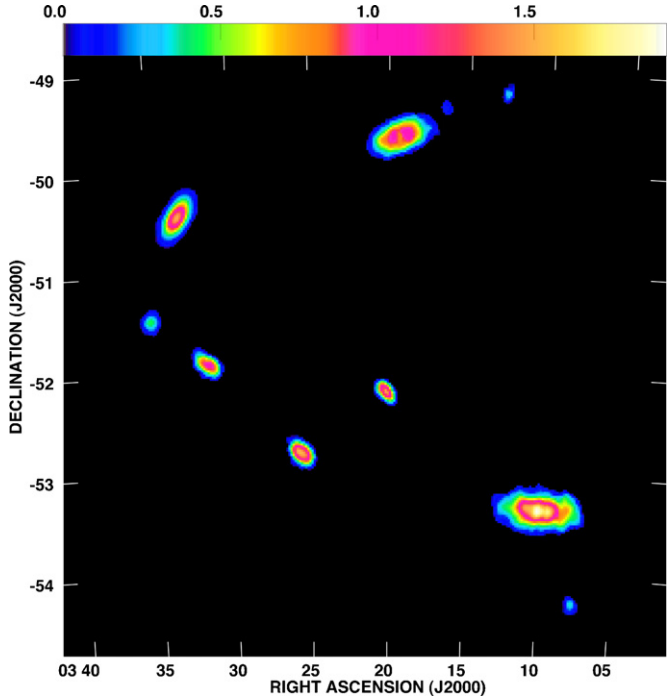

Figure 13. Total H I intensity maps of group galaxies in LGG 93 on the same intensity scale (in units of 10^{21} cm^{-2}). The galaxies have been placed at their correct locations, but have been scaled up in size by a factor of five.

(A color version of this figure is available in the online journal.)

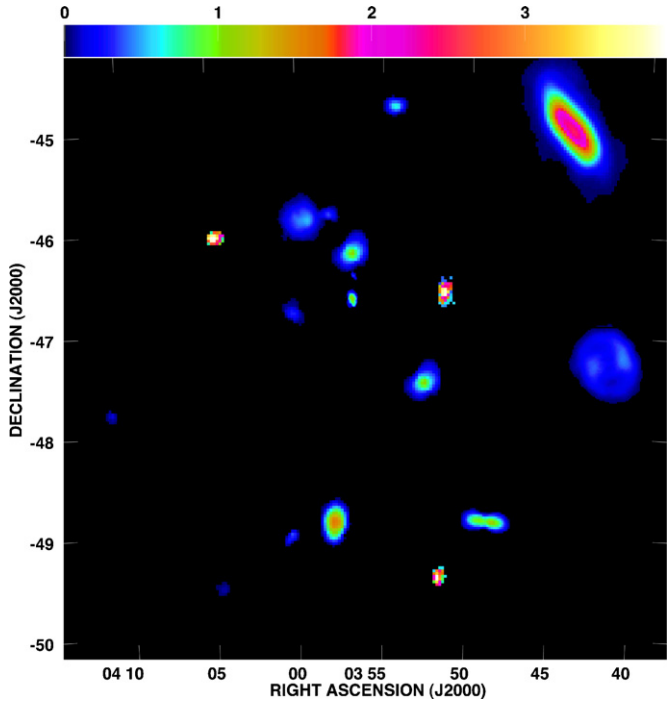

Figure 14. Same as Figure 13, but for LGG 106.

(A color version of this figure is available in the online journal.)

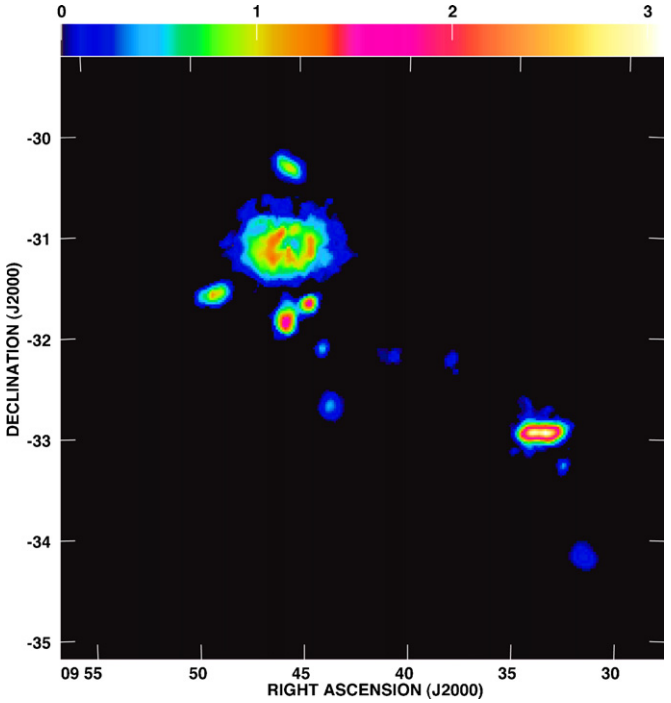

Figure 15. Same as Figure 13, but for LGG 180.

(A color version of this figure is available in the online journal.)

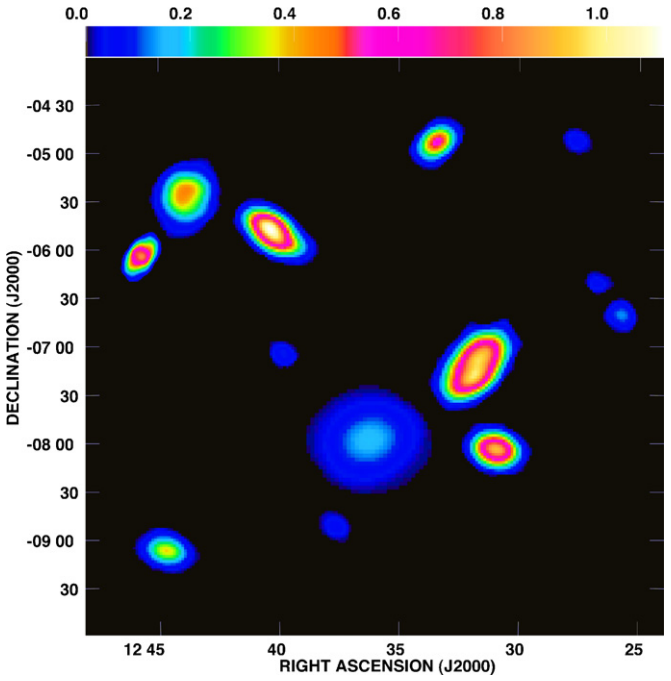

Figure 16. Same as Figure 13, but for LGG 293.

(A color version of this figure is available in the online journal.)

are artificially broadening the velocity width measurements or sources with poor baseline fits.

For the brighter galaxies in our sample, we can also compare our measured parameters with those from HICAT (Meyer et al. 2004). There are a total of 65 sources in our survey that are also in HICAT. The positional uncertainty is 2′ and the robust standard deviation, after discarding those sources more than 10σ from the mean, of V, W_{20}, and $S_{\rm int}$ are 1 km s^{-1}, 4 km s^{-1}, and 0.9 Jy km s^{-1}. For W_{20}, the HICAT widths are systematically larger by $\sim$15 km s^{-1} due to the coarser velocity resolution of HIPASS. The outliers for the HICAT sources are mostly faint sources or those with bad baselines, as for the fake sources, but there was at least one source that was partly confused with another galaxy. Overall, we feel confident that we can accurately measure the properties of the galaxies from their H I spectra.

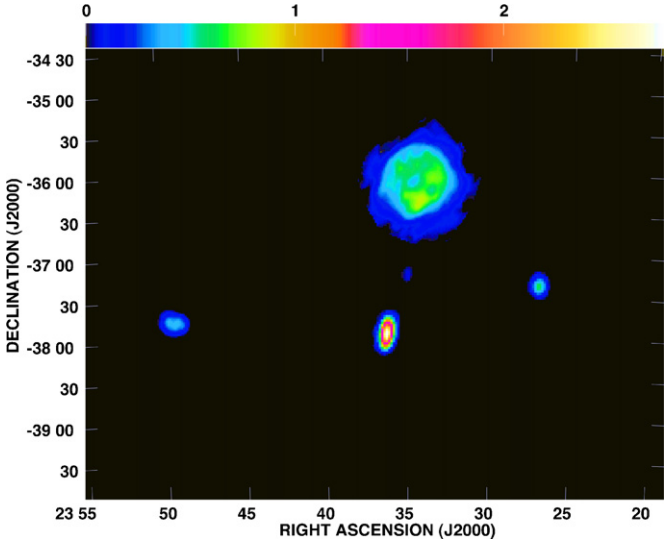

Figure 17. Same as Figure 13, but for LGG 478.
(A color version of this figure is available in the online journal.)

Tables 1 and 2 list the measured H I properties of the confirmed group and background galaxies.

4.3. Group Properties

A total of 31 galaxies detected in our H I survey were previously identified by Garcia (1993) to be associated with the six groups we observed, but how many of the 110 H I-rich galaxies we detected are also associated with the groups? To answer this question, we used an iterative process. Starting with the optical group velocity and velocity dispersion, we identified those H I-detected galaxies within three times the velocity dispersion. The mean recession velocity and velocity dispersion is then recalculated and new group members are identified within 3σ of the central velocity. The process is repeated until both values have changed by less than 1%. The derived values are listed in Table 3. We characterize the radial extent of each group in a few different ways. The diameter of each group is taken to be twice the projected separation of the most distant galaxy from the group center. As we assumed that the groups did not extend beyond our survey area, the diameters tend to be comparable to the diagonal across the survey area. We also calculated the mean projected separation between group galaxies, and the projected radial dispersion of the group galaxies from the optically defined group center. Using this approach, we identified a total of 61 group galaxies in the six groups. Overall, our survey roughly doubled the number of group members found by Garcia (1993). To illustrate the relative locations of the group galaxies, Figures 13–18 show the H I total intensity (moment 0) maps of each group galaxy in its proper location, but scaled up in size by a factor of five.

For each group, we calculated a mass, first assuming that they were virialized:

$$M_{\rm vir} = \frac{3\pi(N-1)}{2G}\frac{\Sigma v_i^2}{\Sigma 1/R_{ij}} \quad (1)$$

from Heisler et al. (1985), where R_{ij} is the projected separation between a pair of galaxies, v_i is the velocity difference between the galaxy and the group velocity, and N is the number of group members. If the groups are not virialized, then we can use the projected-mass estimator to infer their masses:

$$M_{\rm pm} = \frac{32\Sigma v_i^2 R_i}{\pi G(N-1)}, \quad (2)$$

where isotropic orbits are assumed and R_i is the separation between the galaxy and the group center (Heisler et al. 1985). For either mass, we are able to calculate the zero-velocity surface for the bound group:

$$R_0 = \left(\frac{8GT^2M}{\pi^2}\right)^{1/3}, \quad (3)$$

where M is the mass and T is the age of the group (Sandage 1986), taken to be 13.7 Gyr, the age of the universe (Spergel et al. 2003).

In Table 3, we list the derived group properties for each of the six groups. Our selection of the groups as analogs to the Local Group was based purely on the morphology of the galaxies—group members are only spirals and irregulars, the group members being widely spaced, and the absence of detectable intra-group X-ray emission. From Table 3, we see that all of the groups are very similar to each other in terms of extent, morphology, and derived masses. Their average velocity dispersion is 133 ± 59 km s^{-1}; their average diameter is 1.1 ± 0.2 Mpc; and the average separation of the galaxies in the groups is 525 ± 85 kpc. For comparison, we used the measured distances and positions of Local Group galaxies with $M_{\rm H\,I} \geqslant 10^7\,M_\odot$ to calculate a group diameter of ∼3.8 Mpc, a mean galaxy separation of ∼1.3 Mpc, and a radial dispersion of 530 kpc (Mateo 1998; van den Bergh 2000). van den Bergh (2000) report that $\sigma_v = 61 \pm 8$ km s^{-1} for the Local Group. If the groups are all virialized, their median mass is $6 \times 10^{12}\,M_\odot$ with an average zero-velocity surface at 1.5 ± 0.8 Mpc. If the groups are not virialized, then we derive a median mass of $1.3 \times 10^{12}\,M_\odot$ with an average zero-velocity surface of 2.1 ±

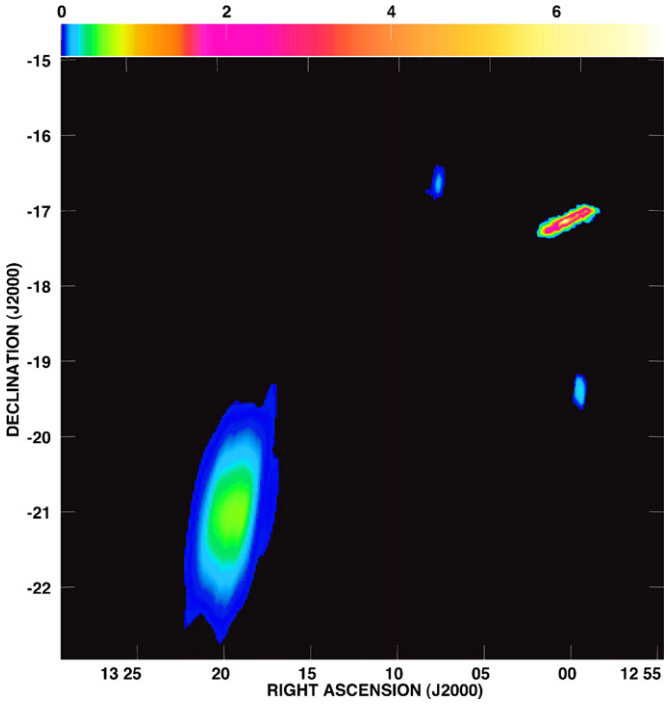

Figure 18. Same as Figure 13, but for the HIPASS group.
(A color version of this figure is available in the online journal.)

Table 1
Group Galaxy H I Detections

Group	Galaxy[a]	α (2000)[b]	δ (2000)[b]	$V_\odot$[c] (km s^{-1})	W_{20}[c] (km s^{-1})	S_{int}[c] (Jy km s^{-1})
LGG 93	NGC 1311	03 20 07.4	−52 11 17	573 ± 2	104 ± 4	14.0 ± 0.1
	IC 1959	03 33 11.8	−50 24 31	639 ± 1	149 ± 2	28.2 ± 0.1
	ESO 200-G45	03 35 01.2	−51 27 09	1026 ± 4	52 ± 8	3.65 ± 0.08
	IC 1914	03 19 25.2	−49 36 11	1029 ± 1	215 ± 2	44.3 ± 0.1
	LSBG F200-023	03 16 28.4	−49 24 02	1045 ± 5	88 ± 10	2.2 ± 0.2
	IC 1954	03 31 32.1	−51 54 17	1062 ± 2	231 ± 4	20.2 ± 0.2
	IC 1896	03 07 52.6	−54 13 01	1076 ± 10	118 ± 20	2.7 ± 0.2
	IC 1933	03 25 39.5	−52 47 04	1060 ± 4	208 ± 8	24.6 ± 0.1
	NGC 1249	03 10 04.6	−53 20 01	1073 ± 1	238 ± 2	99.1 ± 0.2
	AM 0311-492	03 12 42.8	−49 10 58	1308 ± 5	64 ± 10	1.6 ± 0.1
LGG 106	APMUKS B0403-4939	04 04 38.0	−49 30 52	854 ± 2	43 ± 4	0.90 ± 0.07
	ESO 249-G36	03 59 15.6	−45 52 14	898 ± 1	80 ± 2	15.41 ± 0.09
	IC 2000	03 49 08.0	−48 51 26	980 ± 1	280 ± 2	31.9 ± 0.1
	IC 2004	03 51 43.8	−49 25 12	1003 ± 2	126 ± 4	1.3 ± 0.1
	AM 0358-465	03 59 56.6	−46 46 58	1006 ± 2	84 ± 4	3.71 ± 0.09
	ESO 249-G35	03 58 56.3	−45 51 35	1030 ± 3	128 ± 6	5.3 ± 0.1
	NGC 1433	03 42 00.4	−47 13 27	1076 ± 1	184 ± 2	31.1 ± 0.1
	6dF J0351-4635	03 51 33.2	−46 35 49	1029 ± 1	59 ± 2	0.86 ± 0.09
	ESO 201-G14	04 00 27.5	−49 01 39	1052 ± 2	167 ± 4	8.2 ± 0.1
	NGC 1493	03 57 27.9	−46 12 20	1053 ± 1	119 ± 2	41.2 ± 0.1
	NGC 1494	03 57 43.7	−48 54 22	1131 ± 1	183 ± 2	28.9 ± 0.1
	NGC 1483	03 52 47.3	−47 28 38	1149 ± 1	155 ± 2	19.5 ± 0.2
	ESO 201-G23	04 10 52.8	−47 47 10	1197 ± 2	85 ± 4	2.51 ± 0.09
	ESO 249-G32	03 57 21.6	−46 22 05	1039 ± 2[d]	72 ± 7[d]	5.3 ± 0.1[d]
	APMUKS B0355-4643	03 57 08.2	−46 35 00	1169 ± 2[d]	91 ± 13[d]	2.6 ± 0.1[d]
	NGC 1448	03 44 31.0	−44 38 34	1162 ± 4	403 ± 8	20.6 ± 0.3
	ESO 250-G5	04 04 36.6	−46 02 12	1217 ± 2	49 ± 4	0.25 ± 0.10
LGG 180	ESO 373-G7	09 32 45.6	−33 14 40	929 ± 2	230 ± 4	79.8 ± 0.2
	ESO 373-G20	09 43 36.1	−32 44 35	911 ± 2	72 ± 4	9.4 ± 0.1
	UGCA 168	09 33 23.0	−33 02 03	926 ± 2	229 ± 4	61.9 ± 0.1
	ESO 434-G41	09 47 43.5	−31 30 13	988 ± 2	110 ± 4	18.4 ± 0.1
	UGCA 182	09 45 27.9	−30 20 34	998 ± 1	143 ± 2	22.7 ± 0.1
	ESO 373-G6	09 31 51.5	−34 08 13	1048 ± 8	93 ± 16	3.7 ± 0.1
	ESO 434-G19	09 40 44.2	−32 13 45	1033 ± 10	129 ± 8	5.1 ± 0.1
	ESO 434-G17	09 37 57.4	−32 17 20	1132 ± 4	98 ± 8	4.88 ± 0.09
	NGC 2997	09 45 43.8	−31 11 59	1089 ± 1	270 ± 2	191.2 ± 0.2
	UGCA 177	09 44 04.1	−32 10 07	1212 ± 2	97 ± 4	7.0 ± 0.2
	IC 2507	09 44 33.9	−31 47 19	1248 ± 7[d]	153 ± 26[d]	20.8 ± 0.1[d]
	UGCA 180	09 44 46.8	−31 49 13	1250 ± 3[d]	149 ± 3[d]	33.2 ± 0.1[d]
LGG 293	APMUKS B1237-0648	12 39 44.7	−07 05 23	928 ± 2	87 ± 4	2.67 ± 0.09
	UGCA 289	12 35 37.1	−07 52 22	988 ± 2	174 ± 4	26.9 ± 0.1
	NGC 4487	12 31 05.3	−08 03 07	1036 ± 2	213 ± 4	36.6 ± 0.1
	NGC 4504	12 32 18.9	−07 33 55	999 ± 2	243 ± 4	93.9 ± 0.1
	NGC 4597	12 40 11.7	−05 48 17	1036 ± 2	183 ± 4	61.4 ± 0.1
	[KKS2000] 30	12 37 36.3	−08 52 01	1101 ± 1	49 ± 2	1.7 ± 0.1
	LCRSB1223-0616	12 25 38.7	−06 33 30	1244 ± 2[d]	54 ± 3[d]	3.0 ± 0.1[e]
	LCRSB1223-0612	12 25 50.5	−06 29 24	1211 ± 2[d]	50 ± 7[d]	1.3 ± 0.1[e]
	UGCA 286	12 33 37.7	−04 53 12	1290 ± 1	148 ± 2	20.1 ± 0.2
	UGCA 295	12 44 55.0	−09 07 27	1380 ± 4	115 ± 8	8.3 ± 0.3
	APMUKS B1224-0437	12 27 29.2	−04 53 45	1406 ± 2	60 ± 4	2.2 ± 0.2
	DDO 142	12 44 04.1	−05 40 49	1430 ± 1	136 ± 2	38.0 ± 0.2
	DDO 146	12 45 41.1	−06 04 26	1476 ± 1	160 ± 2	16.3 ± 0.2
LGG 478	APMUKS B2332-3729	23 35 05.2	−37 13 19	615 ± 2	49 ± 4	1.14 ± 0.07
	ESO 348-G9	23 49 24.7	−37 46 22	649 ± 1	101 ± 2	13.5 ± 0.1
	NGC 7713	23 36 14.4	−37 56 07	696 ± 2	210 ± 4	62.4 ± 0.2
	IC 5332	23 34 27.4	−36 06 23	701 ± 1	117 ± 2	168.1 ± 0.2
	ESO 347-G17	23 26 56.3	−37 20 35	694 ± 1	88 ± 2	9.32 ± 0.08
HIPASS Group	NGC 5068	13 18 53.8	−21 02 41	670 ± 1	110 ± 2	133.5 ± 0.2
	UGCA 320	13 00 36.8	−17 09 06	742 ± 2	126 ± 4	107.3 ± 0.3
	SGC 1257-1909	12 59 56.0	−19 24 29	828 ± 1	52 ± 2	4.5 ± 0.2
	MCG-3-34-2	13 07 56.6	−16 41 20	958 ± 4	53 ± 8	1.1 ± 0.1

Notes.
[a] These are the names of the optical counterparts to the H I detection based on a search of NED.
[b] Positions are from the ATCA data and have uncertainties of about 10″.
[c] Data are from Parkes H I spectra, except where noted otherwise.
[d] From ATCA spectrum.
[e] Parkes H I flux scaled by ratio of ATCA fluxes.

Table 2
Background Galaxy H I Detections

Foreground Group	Galaxy[a]	α (2000)[b]	δ (2000)[b]	$V_\odot$[c]	W_{20}[c]	S_{int}[c]
LGG 106	ESO 201-G2	03 48 42.7	−48 25 08	1476 ± 2	45 ± 4	1.9 ± 0.1
	IC 1986	03 40 34.7	−45 21 19	1551 ± 2	112 ± 4	11.4 ± 0.2
	LSBG F249-040	03 49 34.9	−46 34 15	1581 ± 4	51 ± 8	0.63 ± 0.15
	IC 2009	03 53 34.6	−48 59 31	1574 ± 2	106 ± 4	6.87 ± 0.09
LGG 293	APMUKS B1237-0724	12 40 16.6	−07 41 05	2219 ± 4	131 ± 8	2.9 ± 0.1
	APMUKS B1236-0417	12 39 01.2	−04 33 35	2413 ± 2	81 ± 4	5.6 ± 0.2
	NGC 4602	12 40 38.1	−05 07 49	2539 ± 4	432 ± 8	35.1 ± 0.2
	FGC 1496	12 44 18.9	−05 32 12	2678 ± 4	209 ± 8	8.2 ± 0.2
	NGC 4626	12 42 27.7	−06 58 10	2800 ± 8[d]	389 ± 16[d]	>13.2 ± 0.2[d]
	HIPASS J1244-08	12 45 12.5	−08 21 09	2886 ± 2	89 ± 4	6.1 ± 0.1
	NGC 4433	12 27 38.9	−08 16 39	∼2977[d]	≳200[d]	>8.3 ± 0.1[d]
LGG 478	ESO 347-G29	23 36 28.2	−38 47 15	1569 ± 1	221 ± 2	30.8 ± 0.1
	NGC 7764	23 50 54.0	−40 43 59	1668 ± 8	213 ± 16	9.4 ± 0.7
	APMUKS B2341-3703	23 44 13.6	−36 46 26	1854 ± 4	57 ± 8	1.35 ± 0.09
	APMUKS B2347-3649	23 50 33.7	−36 33 11	2168 ± 2	95 ± 4	0.93 ± 0.12
	ESO 408-G12	23 37 36.4	−36 59 04	2983 ± 1	201 ± 2	7.3 ± 0.1
	ESO 347-G23	23 34 31.2	−39 31 58	3028 ± 4	144 ± 8	4.5 ± 0.1
	NGC 7713A	23 37 09.8	−37 42 56	3002 ± 2	152 ± 4	7.2 ± 0.1
HIPASS Group	2MASX J1314-2203	13 14 51.7	−22 04 30	1384 ± 4	173 ± 8	6.5 ± 0.3
	UGCA 356	13 26 36.0	−22 14 04	1418 ± 4	133 ± 8	8.7 ± 0.2
	DDO 164	13 06 17.9	−17 30 48	1470 ± 1	95 ± 2	11.0 ± 0.2
	MCG-3-34-67	13 24 15.4	−16 42 16	1494 ± 3	101 ± 6	4.3 ± 0.2
	NGC 5170	13 29 48.2	−17 57 40	1502 ± 1	527 ± 2	79.3 ± 0.6
	LEDA 083827	13 14 30.6	−16 22 30	1487 ± 2	153 ± 4	4.9 ± 0.2
	ESO 576-G25	13 18 29.8	−20 41 08	1560 ± 2	79 ± 4	3.2 ± 0.2
	ESO 575-G61	13 08 14.9	−20 59 58	1642 ± 3	168 ± 6	3.3 ± 0.2
	NGC 5054	13 16 58.7	−16 38 36	1742 ± 2	330 ± 4	23.5 ± 0.2
	UGCA 348	13 19 51.1	−22 16 38	1617 ± 8[e]	177 ± 16[e]	9.2 ± 0.5[e]
	NGC 5134	13 25 18.6	−21 08 09	1758 ± 2	150 ± 4	9.4 ± 0.2
	NGC 5084	13 20 15.6	−21 49 53	1715 ± 4	683 ± 8	106.0 ± 0.4
	2MASX J1324-2015	13 24 54.4	−20 17 45	1732 ± 2	43 ± 4	0.53 ± 0.15
	ESO 576-G42	13 22 01.9	−20 13 19	1885 ± 4	130 ± 8	4.2 ± 0.2
	UGCA 353	13 24 41.8	−19 42 16	1964 ± 4	200 ± 8	17.7 ± 0.2
	ESO 576-G40	13 20 43.6	−22 03 08	1787 ± 4	799 ± 8	50.8 ± 0.4
	IC 863	13 17 13.2	−17 15 07	2514 ± 3[e]	244 ± 6[f]	5.9 ± 0.2[f]
	GALEX 2698124594575839357	13 17 37.1	−17 21 41	2477 ± 7[e]	112 ± 13[e]	3.2 ± 0.2[f]
	SGC 1316-1722	13 18 55.5	−17 38 08	2499 ± 1	109 ± 2	4.7 ± 0.2
	MCG-3-34-4	13 09 43.3	−16 36 14	2569 ± 4	405 ± 8	32.6 ± 0.3
	ESO 576-G11	13 12 54.7[g]	−20 01 29[g]	2757 ± 4	318 ± 8	17.8 ± 0.2
	ESO 575-G53	13 05 05.7	−22 22 49	2644 ± 8	487 ± 16	12.5 ± 0.5
	IC 4237	13 24 40.1[g]	−21 10 39[g]	2661 ± 1	298 ± 2	11.1 ± 0.3
	LEDA 083801	13 13 26.3[g]	−16 03 30[g]	2693 ± 4	166 ± 8	7.9 ± 0.3
	SGC 1317-1702	13 19 55.0	−17 18 50	2686 ± 2	123 ± 4	5.2 ± 0.1
	MCG-3-34-14	13 12 45.1[g]	−17 32 21[g]	2763 ± 4	413 ± 8	19.1 ± 0.3
	LEDA 140150	13 13 26.3[g]	−19 24 21[g]	2780 ± 8	232 ± 16	3.3 ± 0.3
	MCG-3-34-41	13 17 06.2	−16 15 11	2636 ± 2	286 ± 4	5.6 ± 0.3
	ESO 576-G17	13 15 02.3[g]	−17 57 25[g]	2771 ± 1	62 ± 2	3.5 ± 0.1
	MCG-3-34-29	13 03 11.1[g]	−17 17 55[g]	2966 ± 1[d]	63 ± 2[d]	>4.4 ± 0.2[d]

Notes.
[a] These are the names of the optical counterparts to the H I detection based on a search of NED.
[b] Positions are from the ATCA data and have uncertainties of about 10″.
[c] Data are from Parkes H I spectra, except where noted otherwise.
[d] H I profile at the edge of bandpass, so values are highly uncertain or only lower limits.
[e] From ATCA spectrum.
[f] Parkes H I flux scaled by ratio of ATCA fluxes.
[g] From Parkes H I data for those galaxies in HICAT and not confirmed by ATCA observations.

0.8 Mpc. The derived sizes and masses of these loose groups, whether these systems are virialized or not, are all similar to the Local Group with $M_{vir} = (2.3 \pm 0.6) \times 10^{12}\, M_\odot$ and $R_0 = 1.15 \pm 0.15$ Mpc (van den Bergh 2000). As such, we remain confident that these groups are good analogs for the Local Group.

4.4. Galaxy Properties

Interferometer H I total intensity (moment 0) maps overlaid on optical images for all group galaxies are shown in Figures 19–25. H I total intensity contours on optical maps for the background galaxies are shown in Figures 26–30. The properties of the

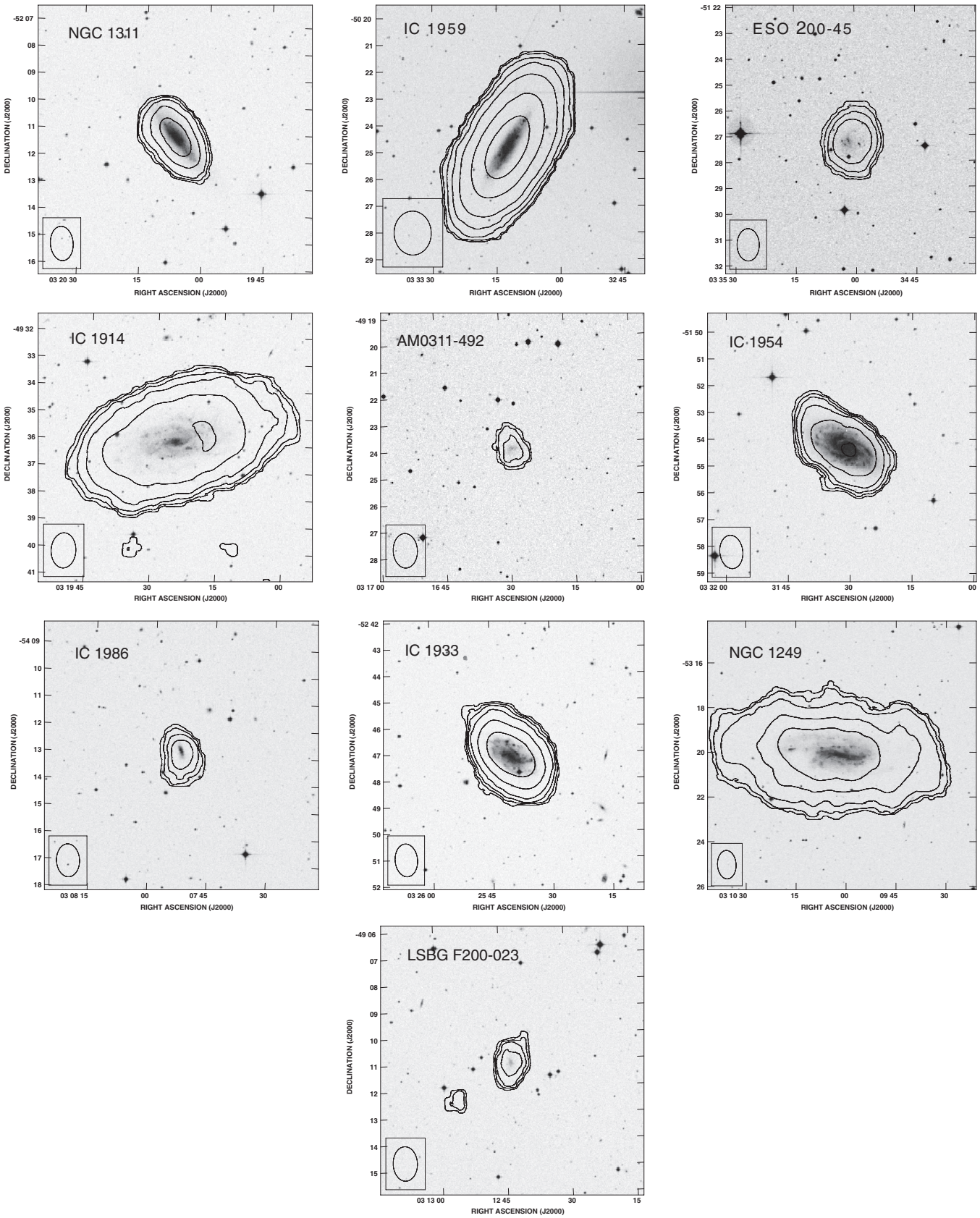

Figure 19. ATCA total H I intensity (moment 0) contours overlaid on second-generation blue Digital Sky Survey gray-scale images for LGG 93 group galaxies. Contour levels are given in Table 4. The beam is shown as the boxed ellipse at the bottom of each image.

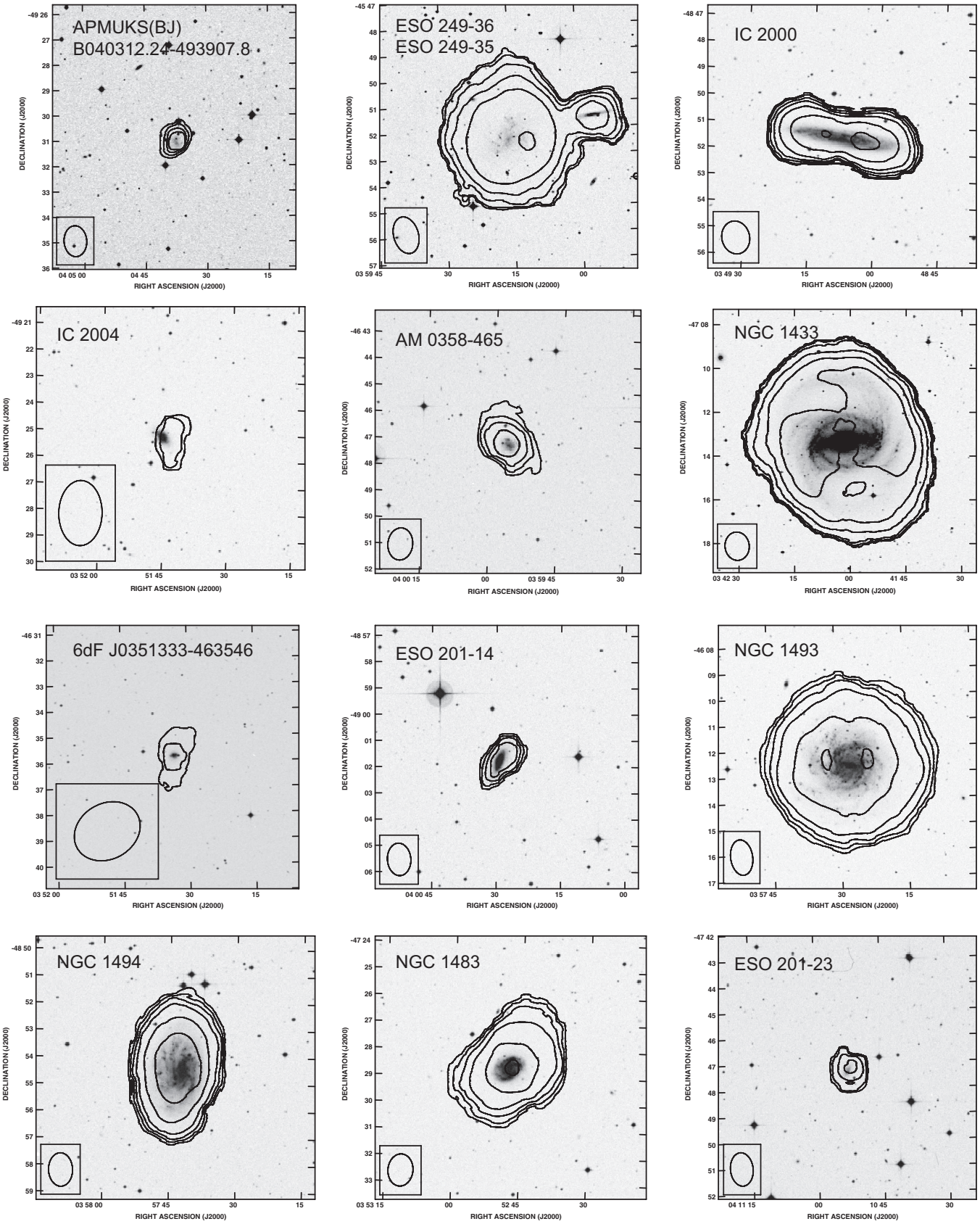

Figure 20. Same as Figure 19, but for LGG 106 group galaxies.

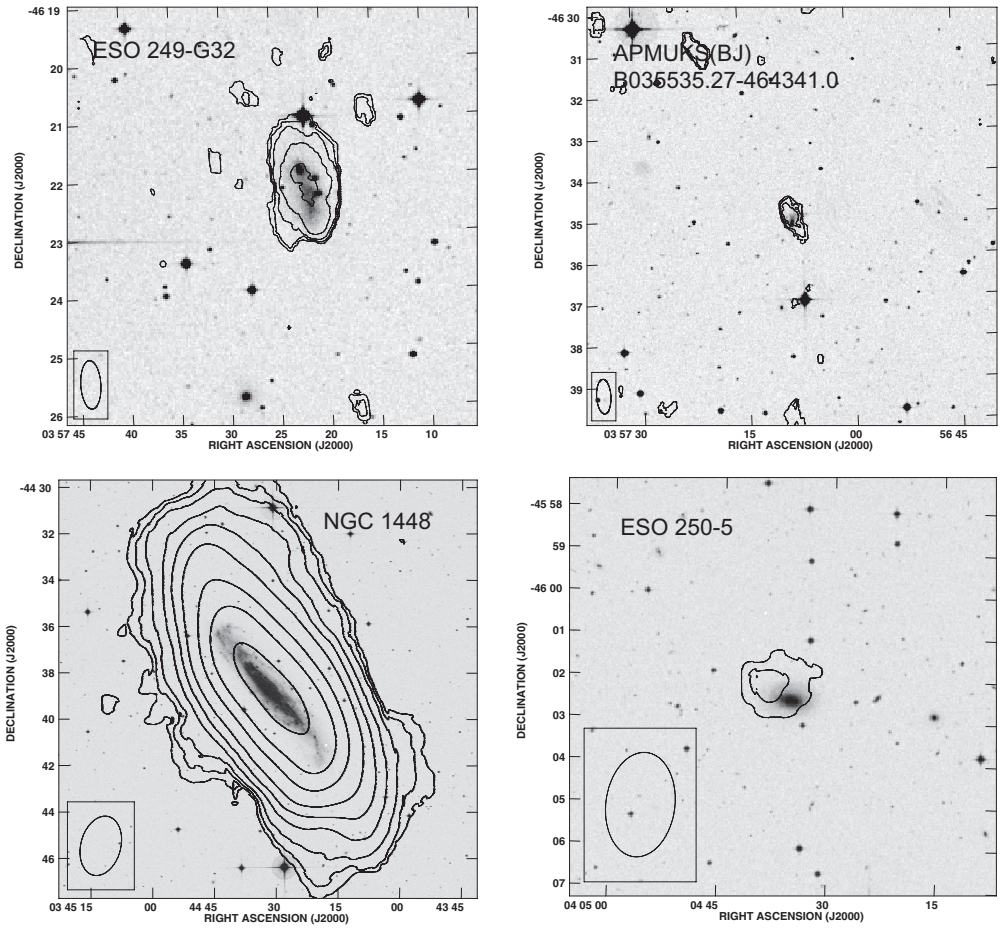

Figure 21. Same as Figure 19, but for the remaining LGG 106 group galaxies.

Table 3
Group Properties

Property	Units	LGG 93	LGG 106	LGG 180	LGG 293	LGG 478	HIPASS Group	Local Group[a]
Distance	Mpc	10.9	13.8	14.8	11.1	8.6	9.1	...
Number of members		10	17	12	13	5	4	21
$V_\odot$[b]	km s^{-1}	989	1061	1064	1194	671	800	...
σ_v[c]	km s^{-1}	218	101	123	191	38	124	61 ± 8[d]
Diameter[e]	Mpc	1.0	1.4	1.2	1.2	0.68	0.92	3.8[f]
Mean galaxy–galaxy separation	Mpc	0.57	0.58	0.49	0.56	0.35	0.60	1.3
σ_r[g]	Mpc	0.48	0.48	0.46	0.45	0.27	0.46	0.53
$M_{\rm vir}$[h]	$10^{12}\,M_\odot$	36 ± 11	4.6 ± 1.1	7.0 ± 2.0	11 ± 3	0.13 ± 0.06	0.51 ± 0.25	2.3 ± 0.6[d]
$R_{0,\rm vir}$[i]	Mpc	2.9	1.5	1.7	2.0	0.45	0.70	1.15 ± 0.15[d]
$M_{\rm pm}$[j]	$10^{12}\,M_\odot$	38 ± 12	12 ± 3	10 ± 3	34 ± 9	0.41 ± 0.18	14 ± 7	...
$R_{0,\rm pm}$[k]	Mpc	3.0	2.0	1.9	2.8	0.65	2.1	...

Notes.
[a] Only those group members with $M_{\rm H\,I} \geqslant 10^7\,M_\odot$ are used to calculate number of members and radii of the Local Group.
[b] The mean recession velocity of the group members.
[c] The rms velocity dispersion of the group members.
[d] From van den Bergh (2000).
[e] Twice the projected separation of the most distant group member from the group center.
[f] The radial separation of GR8 from the Local Group barycenter.
[g] The rms dispersion of the projected radial separations of group galaxies.
[h] Calculated using Equation (1) from Heisler et al. (1985).
[i] Calculated using Equation (3) from Sandage (1986) and $M_{\rm vir}$.
[j] Calculated using Equation (2) from Heisler et al. (1985).
[k] Calculated using Equation (3) from Sandage (1986) and $M_{\rm pm}$.

Table 4
Interferometer Data for Group Galaxies

Galaxy	Beam Size	Channel Width	Noise		Contour Levels[a]
	(arcsec)	(km s^{-1})	(mJy beam^{-1})	(10^{19} cm^{-2})	(10^{19} cm^{-2})
NGC 1311	76 × 50	6.6	5.9	1.1	5,10,20,50,100
IC 1959	98 × 83	6.6	3.4	0.3	1,2,5,10,20,50,100
ESO 200-G45	75 × 51	6.6	3.5	0.7	2,5,10,20,50
IC 1914	78 × 54	6.6	4.0	0.7	2,5,10,20,50,100
LSBG F200-023	78 × 54	6.6	4.0	0.7	2,5,10,20,50,100
IC 1954	75 × 51	6.6	3.7	0.7	2,5,10,20,50,100
IC 1896	73 × 51	6.6	3.7	0.7	2,5,10,20
IC 1933	75 × 51	6.6	3.8	0.7	2,5,10,20,50,100
NGC 1249	76 × 50	6.6	5.4	1.0	5,10,20,50,100
AM 0311-492	78 × 54	6.6	4.0	0.7	2,5,10,20,50,100
APMUKS B0403-4939	73 × 54	3.3	4.9	0.5	2,3,4,5
ESO 249-G36	86 × 57	3.3	3.7	0.3	1,2,5,10,20,50,100
ESO 249-G35	86 × 57	3.3	3.7	0.3	1,2,5,10,20,50,100
IC 2000	75 × 63	3.3	4.0	0.3	1,2,5,10,20,50,100
IC 2004	147 × 98	3.3	5.1	0.1	0.5,1
AM 0358-465	73 × 57	3.3	6.0	0.5	2,6,10,20
NGC 1433	78 × 66	6.6	1.2	0.2	0.5,1,2,5,10,20
6dF J0351-4635	161 × 130	3.3	5.3	0.1	0.5,1
ESO 201-G14	74 × 54	3.3	7.1	0.6	2,5,10,20
NGC 1493	82 × 51	3.3	5.8	0.5	2,5,10,20,50,100
NGC 1494	74 × 53	3.3	6.5	0.6	2,5,10,20,50,100
NGC 1483	73 × 56	3.3	5.8	0.5	2,5,10,20,50,100
ESO 201-G23	77 × 52	3.3	4.8	0.4	1,2,5,10
ESO 249-G32	50 × 21	3.3	4.8	1.7	5,10,20,50,100,200
APMUKS B0355-4643	50 × 21	3.3	4.8	1.7	5,10,20,50,100,200
NGC 1448	157 × 103	6.6	1.7	0.1	0.5,1,2,5,10,20,50,100,200
ESO 250-G5	149 × 98	3.3	4.9	0.1	0.5,1,2,5,10
ESO 373-G7	82 × 55	3.3	8.5	0.7	2,5,10,20,50,100,200
ESO 373-G20	89 × 51	3.3	4.1	0.3	1,2,5,10,20
UGCA 168	82 × 55	3.3	8.5	0.7	2,5,10,20,50,100,200
ESO 434-G41	82 × 55	3.3	10.0	0.8	2,5,10,20,50,100
UGCA 182	93 × 51	3.3	4.1	0.3	1,2,5,10,20,50,100
ESO 373-G6	102 × 81	3.3	3.4	0.2	1,2,5,10,20
ESO 434-G19	99 × 49	3.3	4.7	0.5	2,5,10,20
ESO 434-G17	87 × 55	3.3	7.0	0.5	2,5,10,20
NGC 2997[b]	36 × 29	6.6	0.5	0.35	1,2,5,10,20,50,100
UGCA 177	82 × 55	3.3	9.6	0.8	2,5,10,20,50,100
IC 2507	82 × 55	3.3	8.0	0.6	2,5,10,20,50,100
UGCA 180	82 × 55	3.3	8.0	0.6	2,5,10,20,50,100
APMUKS B1237-0648	155 × 124	3.3	4.1	0.08	0.5,1,2,5
UGCA 289	464 × 349	6.6	5.7	0.03	0.1,0.2,0.5,1,2,5,10
NGC 4487	160 × 125	3.3	4.4	0.08	0.5,1,2,5,10,20,50
NGC 4504	162 × 121	3.3	3.7	0.07	0.5,1,2,5,10,20,50
NGC 4597	158 × 125	3.3	4.2	0.08	0.5,1,2,5,10,20,50,100
[KKS2000] 30	157 × 121	3.3	4.2	0.08	0.5,1,2,5
LCRSB1223-0616	154 × 125	3.3	4.5	0.08	0.5,1,2,5,10
LCRSB1223-0612	154 × 125	3.3	4.5	0.08	0.5,1,2,5,10
UGCA 286	157 × 125	3.3	4.4	0.08	0.5,1,2,5,10,20,50
UGCA 295	155 × 122	3.3	4.3	0.08	0.5,1,2,5,10,20
APMUKS B1224-0437	156 × 125	3.3	4.2	0.08	0.5,1,2,5
DDO 142	155 × 126	3.3	4.6	0.09	0.5,1,2,5,10,20
DDO 146	73 × 53	5.2	1.5	0.2	0.5,1,2,5,10,20,50
APMUKS B2332-3729	123 × 47	3.3	4.1	0.3	1,2,5
ESO 348-G9	90 × 60	3.3	3.3	0.2	0.5,1,2,5,10,20
NGC 7713	111 × 48	3.3	5.0	0.3	1,2,5,10,20,50,100,200
IC 5332	97 × 61	3.3	3.4	0.2	0.5,1,2,5,10,20,50
ESO 347-G17	112 × 50	3.3	5.6	0.4	1,2,5,10,20,50
NGC 5068	680 × 72	13.2	3.6	0.1	0.5,1,2,5,10,20,50
UGCA 320	25 × 18	2.6	1.1	0.7	2,5,10,20,50,100,200,500
SGC 1257-1909	177 × 43	3.3	6.9	0.3	1,2,5,10,20
MCG-3-34-2	208 × 42	3.3	5.3	0.2	0.5,1,2,5,10

Notes.
[a] Corresponding to Figures 19–25.
[b] Data taken from Hess et al. (2009).